Chr21 protein-protein interactions: enrichment in products involved in intellectual disabilities, autism and Late Onset Alzheimer Disease

Julia Viard[1,2*], Yann Loe-Mie[1*], Rachel Daudin[1], Malik Khelfaoui[1], Christine Plancon[2], Anne Boland[2], Francisco Tejedor[3], Richard L. Huganir[4], Eunjoon Kim[5], Makoto Kinoshita[6], Guofa Liu[7], Volker Haucke[8], Thomas Moncion[9], Eugene Yu[10], Valérie Hindie[9], Henri Bléhaut[11], Clotilde Mircher[12], Yann Herault[13,14,15,16,17], Jean-François Deleuze[2], Jean-Christophe Rain[9], Michel Simonneau[1, 18, 19, 20**] and Aude-Marie Lepagnol-Bestel[1**]

[1] Centre Psychiatrie & Neurosciences, INSERM U894, 75014 Paris, France
[2] Laboratoire de génomique fonctionnelle, CNG, CEA, Evry
[3] Instituto de Neurociencias CSIC-UMH, Universidad Miguel Hernandez-Campus de San Juan 03550 San Juan (Alicante), Spain
[4] Department of Neuroscience, The Johns Hopkins University School of Medicine, Baltimore, MD 21205 USA
[5] Center for Synaptic Brain Dysfunctions, Institute for Basic Science, Daejeon 34141, Republic of Korea
[6] Department of Molecular Biology, Division of Biological Science, Nagoya University Graduate School of Science, Furo, Chikusa, Nagoya, Japan
[7] Department of Biological Sciences, University of Toledo, Toledo, OH, 43606, USA
[8] Leibniz Forschungsinstitut für Molekulare Pharmakologie (FMP) & Freie Universität Berlin, Department of Molecular Pharmacology and Cell Biology, Robert-Roessle-Straße 10, 13125 Berlin, Germany
[9] Hybrigenics, 75014 Paris, France
[10] Department of Cellular and Molecular Biology, Roswell Park Division of Graduate School, State University of New York at Buffalo, Buffalo, NY 14263, USA
[11] Fondation Jérôme Lejeune, 37 rue des volontaires, 75015 Paris, France
[12] Institut Jérôme Lejeune, 37 rue des volontaires, 75015 Paris, France
[13] Institut de Génétique et de Biologie Moléculaire et Cellulaire, Illkirch, France
[14] CNRS, UMR7104, Illkirch, France
[15] INSERM, U964, Illkirch, France
[16] Université de Strasbourg, Illkirch, France
[17] PHENOMIN, Institut Clinique de la Souris, ICS; GIE CERBM, CNRS, INSERM, University of Strasbourg, 1 rue Laurent Fries, F-67404 Illkirch-Graffenstaden, France
[18] Laboratoire Aimé Cotton, CNRS, Univ. Paris-Sud, ENS Cachan, Université Paris-Saclay, 91405 Orsay, France
[19] LBPA, Institut d'Alembert, Ecole Normale Supérieure de Paris-Saclay Université Paris-Saclay, 94230 Cachan, France
[20] Department of Biology, Ecole Normale Supérieure de Paris-Saclay Université Paris-Saclay, 94230 Cachan, France

* Co-authors ** Senior co-authors

Correspondence: Simonneau M (michel.simonneau@ens-paris-saclay.fr)

Contribution

JV, YLM, SH, AD, VB, RD, MK, CP, CD, DM, MD, TM and AMLB performed research

JV, YLM, SH, NAE, AD, VB, VP, MS and AMLB analyzed data

PAS, YH, TP, VL, VH, PG, HB, CM, JCR, MS and AMLB designed research

JV, YLM, MS and AMLB wrote the paper

EK, MK, GL, VH, JV, EY, RLH contributed new reagents / new analytical tools

ABSTRACT

Intellectual disability (ID) found in Down syndrome (DS), which is characterized by an extra copy of 234 genes on Chr21 is poorly understood. We first used two DS mouse models that either display an extra copy of the *Dyrk1A* gene or of the mouse Chr16 syntenic region. Exome sequencing of transcripts deregulated in embryonic hippocampus uncovers enrichment in genes involved in chromatin and synapse respectively. Using large-scale yeast two-hybrid screen (154 distinct screens) of human brain library containing at least 10^7 independent fragments, we identified 3,636 novel protein-protein interactions with an enrichment of direct interactors of both Chromosome 21(Hsa21) baits and rebounds in ID-related genes. Using proximity ligation assays, we identified that Hsa21-encoded proteins are located at the dendritic spine postsynaptic density in a protein network located at the dendritic spine post synapse. Hsa21 DYRK1A and DSCAM that confers a ~ 20-fold increase in Autism Spectrum Disorders (ASDs) are part of this dendritic spine postsynaptic network. We found that a DSCAM intracellular domain binds either DYRK1A or DLGs that are multimeric scaffolds for the clustering of receptors, ion channels, and associated signaling proteins. The DYRK1A-DSCAM interaction is conserved from drosophila to humans. The identified postsynaptic.network is enriched in ARC-related synaptic plasticity, ASDs and Late-Onset Alzheimer Disease. Altogether, these results emphasize links between DS and brain diseases with complex genetics.

INTRODUCTION

Down syndrome (DS) is the most common form of intellectual disability (ID), with an incidence of one in 800 births. It is a human genetic disorder, caused by the presence of a third copy of 234 genes from *Homo sapiens* autosome 21 (Hsa21) (1, 2). DS is one of the most complex viable genetic perturbations. In spite of a broad spectrum of clinical symptoms, features common to all DS variants are the intellectual deficit that impairs learning and memory and an increased risk of developing a dementia resembling Alzheimer's disease (AD), even in patients as young as 40 years old (3–5). To date, the precise contribution of each Hsa21 protein overexpression to the cognitive impairment found in DS remains undetermined.

Here, we used two DS mouse models. The first model is a *Dyrk1A* BAC 189N3 model carrying a triplication of the ~152 kb mouse *Dyrk1a* locus containing the whole mouse Dyrk1a gene with a 6 kb flanking fragment on the 5' side and a 19 kb flanking fragment on the 3' side (6). The second model is a transgenic line (Dp(16)1Yey) carrying a triplication of 22.9 Mb from *Mus musculus* chr16 (Mmu16), which are syntenic to 119 genes from Hsa21, including *DYRK1A* (dual-specificity tyrosine phosphorylated and regulated kinase 1A) (7), thus precisely reflecting the gene dosage of Hsa21 orthologs. The *Dyrk1A* gene was found to be a major player in DS whom overexpression induces modifications in synaptic plasticity both in the hippocampus and in the prefrontal cortex (8, 9). Dyrk1a is an important candidate suggested to be involved in the learning and memory impairment seen in DS patients (10), but the regulatory pathways impaired by trisomy of *DYRK1A* remain elusive.

In this work, we examined the respective contributions of *Dyrk1a* and other Hsa21 gene products in pathways linked to ID. Exome sequencing of transcripts mis-regulated in the embryonic hippocampus uncover two contrasting repertoires of genes: chromatin related genes for the *Dyrk1A* trisomy model and a synapse related genes for the Dp(16)1Yey model. In order to gain further insight into the molecular network of proteins responsible for DS phenotypes, we next searched for human brain proteins that interact with proteins encoded by Hsa21. To this end, we conducted a large-scale yeast two-hybrid screen using Hsa21 baits and a human brain library of targets. This analysis revealed that both direct interactors of Hsa21-encoded proteins and their direct rebounds are enriched in proteins involved in ID. Moreover, we found an enrichment in HSA21-encoded proteins that are part of a network located in dendritic spine postsynaptic density. The same interactome is also enriched with proteins involved in ARC-related synaptic plasticity, Autism Spectrum Disorders and Late-Onset Alzheimer Disease (LOAD).

RESULTS

Whole-genome RNA sequencing and quantitative proteomics reveal two contrasted networks of deregulated genes of hippocampus from 189N3 *DYRK1A* and Dp(16)1Yey DS models

Figure 1.

Figure 2.

Supplementary Table S1

Supplementary Table S2

We used the 189N3 and the Dp(16)1Yey/+ DS mouse models. We performed RNA sequencing on embryonic E17 hippocampi of these two DS models. We identified 84 deregulated genes in 189N3 mice (**Supplementary Table S1**) and 142 deregulated genes in Dp(16)1Yey/+ (**Supplementary Table S2**) compared to their littermate controls.

Gene ontology (GO) Process analyses of differentially expressed genes revealed a deregulation of chromatin proteins for 189N3 mice with:

GO:0006334~nucleosome assembly (P value=1.17 e^{-08})

GO:0031497~chromatin assembly (P value= 5.98 e^{-08})

GO:0034728~ nucleosome organization (P value = 1.71 e^{-07}).

Deregulation of chromatin proteins is in agreement with data that previously reported by us (11, 12).

In contrast, for Dp(16)1Yey/+, we found a deregulation of proteins involved in synaptic function:

GO:0007268~chemical synaptic transmission (Pvalue= 6.87e-^{09})

GO:0051932~synaptic transmission, GABAergic (Pvalue= 1.27e-^{05})GO:0048812~neuron projection morphogenesis (Pvalue= 8.24e-^{05})

Interestingly, for the GO:0051932~synaptic transmission, GABAergic, 6 of 77 genes are deregulated for a repertoire of 53 out of 24850 human genes (7.8%), indicating an enrichment of 36.54 fold compared to expectations (hypergeometric P-value = 1.48 e-^{08}). This result is in full agreement with the impairment of excitation-inhibition balance (E–I balance) in synaptic activity found in DS (13, 14).

First, we used Dapple analysis (15) of 189N3 and Dp(16)1Yey/+ differential expressed genes to evidence two contrasted networks with statistically significance (direct edge counts; $p<0.05$) showing that genetic variation induced by the triplication of the mmu16 affects a limited set of underlying mechanisms (**Figure 1 A-B**). We next used Webgestalt. Suite (16) for the142 deregulated genes in Dp(16)1Yey/+ with 77 upregulated and we identified two significant networks (A) and (B). **A**: a network that includes 8 genes from the 70 upregulated list with an enrichment in GO Biological Process: chemical synaptic transmission (p=220446e-16). **B**: a network that includes 4 genes from the 77 upregulated list with an enrichment in GO Biological

Process: Biological Process: glutamate receptor signaling pathway (p=220446e-16). Note that three genes (*Camk2a*, *Gda*, *Dlgap3*) are part of a protein network of ARC-dependent DLG4 interactors that include 20 proteins (17), indicating an over enrichment of 43.85 fold compared to expectations (hypergeometric p-value = 4.20 e-05) [Parameters: 3, 20, 77, 22,508 number of mouse genes from Mouse Ensembl (GRCm38.p6)].

Altogether, these results indicate a contrasted deregulation of chromatin-related genes for 189N3 model and synaptic plasticity-related genes with a n enrichment in genes linked to ARC postsynapse Complexes Involved with Neural Dysfunction and Intelligence for Dp(16)1Yey/+ model.

Establishment of a Hsa21 protein-protein interaction map by a high-throughput, protein domain-based yeast two-hybrid (Y2H) screening

Figure. 3.

Figure. 4

To improve our knowledge of the molecular network underlying DS, we performed a large-scale protein-protein interaction study. We performed 72 screens with HSA21 protein as baits and 82 screens against their direct interactors (rebounds) using a highly complex random-primed human adult brain cDNA library. We identified 1687 and 1949 novel direct interactions (**Figure 3 A-D**). These interactions were ranked by category (a to f), using a Predicted Biological Score (PBS) (18). Analysis of direct interactors from 72 HSA21 baits screens gives 1687 novel interactions identified with 76 already known (Biogrid) interactions confirmed (**Figure 3A-B**). Analysis of direct interactors from 82 rebound screens gives 1949 novel interactions were identified with 97 already known (Biogrid) interactions confirmed (**Figure 3 C-D**). We next compared these direct interactors with three lists of genes involved in intellectual disability (19, 20). Both HSA21 direct interactors (**Figure 3 E**) and rebound direct interactors (**Figure 3 F**) are enriched in ID proteins (p= VVVV and p=, respectively) suggesting that these two types of interactors are part of a large ID network. The whole set of PPI data has been deposited at INTACT database.

We realized a biological processes analysis using GO DAVID (see methods) (**Figure 4**). The colored nodes correspond to the most significant results with GO:0022008~Neurogenesis (*p*-value=3.06e-17); GO:0048812~Neuron projection morphogenesis (*p*-value=, 2.91e-13); GO:0050767~Regulation of neurogenesis (*p*-value=2.66e-06); GO:0043632~Modification-dependent macromolecule catabolic process (*p*-value=6.46e-05); GO:0051962~Positive regulation of nervous system development (*p*-value=6.29e-06); GO:0045665~Negative

regulation of neuron differentiation (*p*-value=1.55e-07). Altogether, our data indicate an enrichment of interactions related to neuronal differentiation.

Linking HSA21 proteins to Late Onset Alzheimer Disease (LOAD) and neuropsychiatric diseases: DSCR9-CLU, DYRK1A-RNASEN

Figure 4

Supplementary Figure1

We first focused our analysis to two novel interactions with a potential importance in brain diseases, by combining Yeast two Hybrid (Y2H) interaction data with proximity ligation assays (PLA) that allow to localize PPI at the subcellular level when the maximal distance between the antibodies required for producing a signal is 40 nm (21).

The two selected PPI links respectively HSA21 DSCR9 gene with CLU, a risk factor for Late-Onset Alzheimer Disease (LOAD), HSA21 DYRK1A with RNASEN, a microprocessor complex subunit (**Figure 4A**).

As no *bona fide* antibody was available, we generated a GFP DSCR9 construct, in order to image DSCR9 protein. PLA evidenced nuclear localization of this novel interaction between DSCR9 and CLU. Using in situ PLA, we identified PPI inside nuclei on primary cortical neurons using anti-GFP and anti-Clu antibodies (**Figure 4B**). DSCR9 and DSCR10 have been identified as genes that appeared exclusively in primates such as chimpanzee, gorilla, orangutan, crab-eating monkey and African green monkey and are not present in other non-primate mammals (22) (**Supplementary Figure 1**). CLU gene was identified as one of the 20 LOAD genetic risks (23) and confirmed in a recent meta-analysis a large genome-wide association meta-analysis of clinically diagnosed LOAD (94,437 individuals) (24). Our results indicate a direct nuclear interaction between the product of a HSA21 gene that contributes to the genomic basis of primate phenotypic uniqueness and a LOAD risk gene.

For DYRK1A-DGRC8 interaction, we first validated this interaction by immunoprecipitation using native conditions (no overexpression) in EK293 cells (**Figure. 4C**). Localization of the interaction in neuronal nuclei was evidenced by PLA on primary cortical neurons transfected at DIC5 with Dyk1a-GFP construct, using anti-GFP and anti-Rnasen antibodies (**Figure. 4D**).

The Microprocessor complex is a protein complex involved in the early stages of processing microRNA (miRNA) in animal cells. The complex is minimally composed of the ribonuclease enzyme Drosha and the RNA-binding protein DGCR8 (also known as Pasha) and cleaves primary miRNA substrates to pre-miRNA in the cell nucleus (25).

Deficiency of Dgcr8, a gene disrupted by the 22q11.2 microdeletion that gives a schizophrenia phenotype in humans, results in altered short-term plasticity in the prefrontal cortex (26). One

can suppose that functional phenocopies of this DGC8 haploinsufficiency may occur by titration of its partner RNASEN when DYRK1A is overexpressed. As alterations of the microRNA network cause neurodegenerative disease (27), our results suggest that DYRK1A-RNASEN interaction could have direct relevance for our understanding of early AD in DS persons.

Interactome of Hsa21 proteins located in the postsynaptic compartment of the dendritic spine

Figure 5

Supplementary Figure 2

We next wanted to validate PPI identified by Y2H and to define the subcellular localization of the interactions, using proximity ligation assays. Our working hypothesis was that a subset of Hsa21 proteins and their interactors could be located at the level of dendritic spine. We defined a putative synaptic network (**Figure 5A**) based on the Y2H that we identified and their position in a four layers model as proposed by (28, 29). The four layers involve (i) a membrane layer for ionic channels, neurotransmitter receptors and cell-adhesion molecules, (ii) a second layer for DLGs, (iii) a third layer for DLGAPs and (iv) a fourth layer for direct DLGPs interactors (such as SHANKs). Validation of the synaptic network was done using PLA.

We were able to quantify dendritic spine postsynapse localization for 21 PPI identified by Y2H, with 13 novel PPIs (GRIK1-HCN1, GRIK1-KCNQ2, GRIK1-SEPT7, GRIK1-KALRN, HUNK-AGAP3, HUNK-SYNPO, HUNK-LIMK1, TIAM1-BIN1, TIAM1-DLG1, KCNJ6-DLG4, KCNJ6-DLG2, DSCAM-DLG4, DSCAM-DLG2) and 8 already known PPI but without any subcellular distribution data (GRIK1-DLG4, KCNJ6-DLG1, ITSN1-SNAP25, ITSN1-DLGAP1, SIPA1L1-DYRK1A, SIPA1L1-DLG4, DLG2-GRIN2A,DLG2-GRIN2B).

We first focused on protein-protein interactions of Hsa21 GRIK1 (**Figure 5B**). This protein is one of the GRIK subunits functioning as a ligand-gated ion channel. Kainate receptors (KARs) are found ubiquitously in the central nervous system (CNS) and are present pre- and post-synaptically (30). We first identified the GRIK1-KCNQ2 interaction. As KCNQ2 potassium channels are known to functionally interact with HCN1 potassium channels in prefrontal cortical dendritic spines (31), we validated that HCN1, KCNQ2 and GRIK1 physically interact in dendritic shafts and spines using PLA and found a direct interaction between GRIK1 and HCN1 in these compartments. We also identified and validated interactions between GRIK1 with SEPT7 and KALRN. SEPT7, a member of the septin family of GTPases, is localized to dendritic branching points and spine necks (32). KALRN is a Rho-GEF exclusively localized to the postsynaptic side of excitatory synapses (33) and binds NMDA receptor subunit Nr2b

(Grin2b) (34). These results suggest that GRIK1 is part of two synaptic complexes, one located near PSD-95 (DLG4) at the tip of the dendritic spine and the other at the neck of spines.

Hsa21 HUNK (alias MAK-V) was found in the Y2H screen to interact with the GTPase-activating protein AGAP3, the actin-associated protein Synaptopodin (SYNPO) and the synapse related LIMK1. These three interactions were validated at the level of synapse using PLA (**Figure 5C**). AGAP3 was recently identified as an essential signaling component of the NMDA receptor complex that links NMDA receptor activation to AMPA receptor trafficking (35). SYNPO was localized to necks of dendritic spines and linked to the spine apparatus, assumingly playing an essential role in regulating synaptic plasticity (36). These results suggest that HUNK is involved in complexes localized both near PSD-95 and the spine apparatus. *LIMK1* functions in intracellular signaling and is strongly expressed in the brain, with hemizygosity suggested to impair visuospatial constructive cognition (37).

We next analyzed Hsa21 TIAM1 interaction with BIN1 and DLG1. TIAM1 is a Rac1 associated GEF 1, involved in synaptic plasticity (38) and specifically expressed in subgroups of glutamatergic synapses such as dendritic spines of the performant path-dentate gyrus hippocampal synapse (39) (**Supplementary Figure 2**) . BIN1 is the second risk factor, after APOE4, identified by Genome Wide Association Studies (GWAS) in LOAD (23, 24). BIN1 protein has multiple functions, including a role at the postsynapse (40, 41). Using PLA, we evidenced TIAM1-BIN1 and TIAM1-DLG1 interactions at the level of dendritic spines (**Figure 5C**).

Another set of noteworthy interactions identified in the Y2H screen (**Figure 5A**), as well as validated via PLA (**Figure 5D**), is between Hsa21 potassium channel KCNJ6, a voltage-insensitive potassium channel member of the kainate ionotropic glutamate receptor (GRIK) family, and three DLG members: DLG1, DLG2 and DLG4. We also found an increase in the number of KCNJ6-DLG2 interactions in the Dp(16)1Yey transgenic mouse model, compared to the control. In contrast, the number of GRIN2A/B-DLG2 interactions was unchanged (**Figure 5D**). *KCNJ6* is expressed in dendrites and dendritic spines at the PSD of excitatory synapses (42, 43) and its trisomy induces synaptic and behavioral changes (44).

Two interesting interactions detected in the Y2H screen (**Figure 5A**) and validated via PLA (**Figure 5E**) are between Hsa21 Intersectin (ITSN1) and both SNAP25 and DLG-Associated Protein 1 (DLGAP1/GKAP). SNAP25, a member of the SNARE protein family, is not only essential for the exocytosis of synaptic vesicles (45), but involved in trafficking of postsynaptic NMDA receptors (46) and spine morphogenesis (47). DLGAP1 is a core protein of the scaffolding complex of the synapse (48). These results are in agreement with the *Itsn1* mutant mice phenotype that is characterized by severe deficits in spatial learning and contextual fear memory (49) and in synaptic hippocampal plasticity (50).

SIPA1L1, also known as SPAR is a Rap-specific GTPase-activating protein (RapGAP), a regulator of actin dynamics and dendritic spine morphology, leading to its degradation through the ubiquitin-proteasome system (51, 52). Here, we evidenced direct interaction between SIPA1L1 and DYRK1A or DLG4 (**Figure 5F**) DYRK1A and DLG4

We also identified the location of the Y2H interactions of DSCAM with DLG2 (Discs large 2) and DLG4 at the dendritic spines, using PLA (**Figure 5G**). Then, using DSCAM as bait against single DLG family members (one-by-one Y2H approach), we identified interactions between DSCAM and the four members of the DLG family: DLG1, DLG2, DLG3, and DLG4 (**Figure 5G-H**). DSCAM is known to regulate dendrite arborization and spine formation during cortical circuit development (53). DLG1 (alias SAP97), DLG2 (alias PSD93/chapsyn-110) and DLG4 (alias PSD-95/SAP90) are known to bind various proteins and signaling molecules at the postsynaptic density (PSD) (54, 55). Intriguingly, mice lacking *Dlg2* and people with *Dlg2* mutations display abnormal cognitive abilities (56).

Altogether, our results demonstrate location of novel proteins in the nanoscale region that corresponds to the four layers of the dendritic spine and covers a 75 nm-thick region from synaptic cleft (57).

DSCAM-DYRK1A interaction

Figure 6

In our Y2H screens, we identified interactions between human DSCAM, its human paralog DSCAML1 and human DYRK1A. This interaction occurs in the same intracellular domain (45 amino acids) of these cell adhesion molecules (**Figure 6A**). Furthermore, their drosophila homologs, DSCAM4 and minibrain (MNB), were also found to interact in the same phylogenetically conserved domain of 45 amino acids (**Figure 6B**). We confirmed human DSCAM-DYRK1A interaction by immunoprecipitation, using adult mouse cortex (**Figure 6C**). We were unable to find an anti DYRK1A antibody that can be used for PLA proximity ligation assay. We used preparation of synaptosomes and immunoprecipation to evidence DSCAM-DYRK1A interaction in this subcellular fraction (**Figure 6D-E**). We found that DSCAM interacts with DLG4 and DLG2 in the postsynapse, using PLA (**Figure 5G**). Altogether, our data indicate that DSCAM-DYRK1A and DLGs interacts in the postsynapse. To the best of our knowledge, this is the first localization of DSCAM and DYRK1A in the postsynapse.

Both DSCAM and DYRK1A are part of a subset of 30 genes that confers 20-fold risk in autism-spectrum disorders (ASDs). In ASD, studies leveraging the statistical power afforded by rare de novo putatively damaging variants have identified more than 65 strongly associated genes (58). The most deleterious variants (likely gene disrupting or LGD) in the highest confidence

subset of these genes (N = 30) as a group confer approximately 20-fold increases in risk, with LGD variants in the highest confidence genes carrying even greater risks (59).

A synaptic network enriched in Hsa21 proteins, ASD high-risk genes, ARC-related protein network and Late Onset Alzheimer Diseases (LOAD) risk factors

Figure 7

We summarized our PPI data at the synapse with a protein network of 28 products (**Figure 7**). This synaptic network is enriched in HSA21 proteins with 5 out 234 HSA21 gene products (the results are enriched 18.72 fold compared to expectations; hypergeometric p-value = 6.435 e-07). This 28 proteins network is also enriched in high-risk ASDs genes. We found that DSCAM and DYRK1A are part of this network that includes also DLGAP1 and SHANK3. These four genes are considered to confer ~20-fold increases in risk, for a group containing 30 genes (58, 59). The enrichment here is 97.35 fold compared to expectations (hypergeometric p-value = 7.52e-08; parameters: 4, 28, 30, 20444).

[234/ Ensembl release 88 - Mar 2017]

The third group of enrichment is an ARC-dependent postsynaptic complex involved with Neural Dysfunction and Intelligence (17). This group includes 20 proteins and 7 of them (Grin2a, Grin1, Dlg4, Dlg2, Dlgap1, Syngap1, Camk2a) are part of our synaptic complex (the results are enriched 255.55 fold compared to expectations; hypergeometric p-value = 3.06e-16; parameters: 7, 28, 20, 20444). The fourth group is Late-onset (LOAD) that involve 11 new loci corresponding to 26 candidate genes, (23, 60). We found an enriched 112.33 fold compared to expectations (hypergeometric p-value = 4.12e-08; parameters: 4, 28, 26, 20444).

Altogether, these results demonstrate that our postsynaptic network is enriched in Hsa21 proteins, ASD high-risk genes, ARC-related protein network and LOAD risk factors.

Discussion

In spite of the availability of various mouse DS models, cognitive impairment phenotypes found in DS have not been related to specific alterations of molecular pathways. Furthermore, to the best of our knowledge, no specific pathways linked to synaptic alterations have been described in models overexpressing a given chr21 gene as compared to models overexpressing a syntenic region.

In the present study, we analyzed molecular changes in the hippocampus of two mouse DS models. We found molecular changes linked to chromatin remodeling in the Dyrk1A BAC 189N3 mice. In contrast, expression of an extra copy of the entire Hsa21 syntenic region, spanning 22.9 Mb and containing 115 Hsa21 gene orthologs, including *Dyrk1A*, on Mmu16 in the Dp(16)1Yey transgenic mouse model, induced changes in GO glutamatergic and gabaergic synaptic transmission pathways.

Using large scale Y2H we evidenced that both direct interactors (n=1687) and their second order interactors that we capture using our rebound screen (n=1949) are enriched in ID genes. This observation suggests that protein-protein complexes that includes a Hsa21 protein are at-risk complexes for ID.

The PLA approach that allows localizing Protein-Protein Interactions in a given subcellular comportment allows us to focus on synaptic compartment where subtle deregulations may occur (61, 62).

We identified that interactions at the synapse are enriched in Hsa21 gene products. In particular, we were able to demonstrate that both DYRK1A and DSCAM are part of the postsynapse. DYRK1A and DSCAM are high-risk genes for ASDs with a 20 fold increase as compared to the general population (58, 59). Gene dosage changes of both DYRK1A and DSCAM may involve distinct molecular mechanisms as compared to those occurring in ASDs and linked to damaging mutations. Further work to decipher these molecular changes can illuminate both DS and ASDs pathophysiology.

We also characterized a significant enrichment in ARC-dependent synaptic network involved in intelligence and brain diseases (17). Mutations disrupting this molecular hierarchy can change the architecture of synaptome maps, potentially accounting for the behavioral phenotypes associated with neurological and psychiatric disorders (61). Further work will be needed to analyze the changes in protein complexes at the synapse, when gene dosage changes for partners of these complexes.

It is well documented that Down syndrome, caused by trisomy of chromosome 21, is the single most common risk factor for early-onset Alzheimer's disease. Triplication of APP has been as considered as a candidate for this phenotype but trisomy of human chromosome 21 enhances

amyloid-β deposition independently of an extra copy of APP indicating that triplication of chromosome 21 genes other than APP is likely to have an important role to play in Alzheimer's disease pathogenesis in individuals who have Down syndrome (63). We reported here an enrichment in LOAD genes identified by GWAS strategies, with RIN3, BIN1 and CASS4 in our postsynaptic network. We (40) and other (41) characterized BIN1 at the level of the synapse using super-resolution microscopy. Other protein networks that includes BIN1 and CASS4 have been reported in microglia (64). Altogether, these results suggest that cell-distinct proteins complex may contribute to Alzheimer phenotype in DS.

Interestingly, from our Y2H and PLA approaches, we identified novel candidates in the postsynaptic domain that we characterized by four layers as in (28, 29) has a very restricted width in the range of 75 nm (57). Super-resolution microscopy approaches recently revealed that spine synapses *in vitro* and brain slices nanodomains that form a trans-synaptic column and contain discrete, precisely aligned sub-diffraction nanomodules, whose number, not size, scales with spine volume (65, 66).

Changes in stoichiometry of interactors, as expected for Hsa21 proteins may modify the functional impact of a given protein complex. The report that a same Neuroligin4 mutation can generate either ID or high-level ASD supports such subtle changes (67). Similarly, some protein complexes may integrate only a given form of a protein, as it is the case for TIAM1 in glutamatergic synapses from entorhinal cortex (39).

Together, our results suggest that protein-protein interactions identified here can be part of different dendritic spine signalosomes deregulated by three doses of Hsa21 proteins.

In conclusion, our results provide the first report, to our knowledge, of differential impacts of chromosome 21 *DYRK1A* on chromatin remodeling and of the 115 Hsa21 gene orthologs including *DYRK1A*, on synapse function. Our results exemplify the link of DS to other forms of ID and to degenerative diseases displaying complex genetics such as LOAD. The molecular pathways studied here can promote the development of novel therapeutic targets to treat cognitive impairments found in DS.

MATERIALS AND METHODS

Animals and genotyping

We used wild-type mice of the OF1 strain for neuronal primary culture, of the C57BL6 strain and 189N3 or Dp(16)1Yey transgenic line for neuronal primary cultures. Genotypes were determined using genomic DNA extracted from skeletal muscle fragments and the PCR protocol and primers as described previously (Lepagnol-Bestel et al., 2009).

Primary cell cultures

Primary cultures from OF1 mice were performed as described in Loe-Mie et al., 2010. Heterozygous 189N3 or Dp(16)1Yey mice were crossed with C57BL6, resulting in embryos of transgenic or wild type genotypes. E15.5 189N3 or Dp(16)1Yey cortical neurons were dissociated by individually dissecting each embryo out of its amniotic sac, removing the head and dissecting out the target brain tissue in an separate dish. The remainder of the brain was used for genotyping. Neurons from each embryo were dissociated enzymatically (0.25% trypsin), mechanically triturated with a flamed Pasteur pipette, and individually plated on 24-well dishes (1×10^5 cells per well) coated with poly-DL-ornithine (Sigma), in DMEM (Invitrogen) supplemented with 10% fetal bovine serum. Four hours after plating, DMEM was replaced by Neurobasal® medium (Invitrogen) supplemented with 2mM glutamine and 2% B27 (Invitrogen). For nuclear interactions or dendritic interactions, cortical neurons were analyzed after 7 days or 21 days in culture respectively.

Constructs

Mouse Dyrk1a cDNA was cloned in GFP plasmid as described (Lepagnol-Betel et al. 2009). Human USP25 and SYK were cloned in GFP and MYC plasmids respectively as described (Cholay et al. 2010). Human GDI1 and DSCR9 were amplified by PCR from IMAGE: 4156714 and IMAGE: 6065320 cDNA clones, respectively (SourceBioscienes) with the following primers:

GDI1 forward: 5'-gatcggccggacgggccGACGAGGAATACGATGATCGTG

GDI1 reverse: 3'-gatcggccccagtggccTCACTGCTCAGCTTCTCCAAAGACGTC

DSCR9 forward: 5'-gatcggccggacgggccATGGGCAGGATTTGCCCCGTGAAC

DSCR9 reverse: 3'-gatcggccccagtggccTCACCATAATTCCTGTGTCTGAATCTGAA

The SfI digestion products of the amplicons were inserted into the multiple cloning site of the HA and GFP expression vectors respectively under control of the CMV promoter.

Primary cell cultures and transfection

Cortical primary neurons were cultured as described above. At DIC5, the cells were transfected with constructs using Lipofectamine 2000 (Invitrogen), as described by the manufacturer. Cells were analyzed 48 hours after transfection at DIC7.

HEK293 cell cultures and transfection

HEK293 cell line were plated in 24-well plates in DMEM (Invitrogen) supplemented with 10% fetal bovine serum. At 70% confluency, the cells were transfected with constructs (co-transfections were performed at 1:3 ratio) using Lipofectamine 2000 (Invitrogen), as described by the manufacturer. Cells were analyzed 48 hours after transfection.

***In situ* proximity ligation assays (PLA) and microscopy**

Cells were fixed by incubation for 20 min at room temperature in 4% paraformaldehyde in phosphate-buffered saline (PBS), permeabilized by incubation for 10 min at room temperature in 0.3% Triton X-100 in PBS, washed two times within PBS and PLA was realized according to the instructions of the manufacturer (DuoLink, Sigma). Primary antibodies used were as shown in Supplementary Table S3. For the analysis of PLA interactions points, cells were scanned using the laser scanning confocal microscope (Leica, SP5 from PICPEN imagery platform Centre de Psychiatrie et Neuroscience) at 63× magnification, and Z-stacks were build using the ImageJ software (Wayne Rasband, NIH). Nuclear PLA interaction number was manually counted inside the nuclear body and normalized with the nuclear area of each neuron. Synaptic PLA interaction number was manually counted on 150 µm long dendritic segments starting after the first branch point in the dendritic tree. One 150 µm dendritic segment per neuron was analyzed.

Statistical analysis

The analyses performed on transgenic neurons with at least 3 embryos and at least 10 cells per embryo for synaptic and nuclear analyses. The analyses performed on OF1 neurons with at least 3 different cultures and at 8 cells and 14 cells per culture for synaptic and nuclear analyses respectively. The analyses performed on HEK293 cells with at least 3 different transfections and 5 cells per transfection for nuclear or cytoplasmic analyses. T-tests were performed with Excel Software.

Quantitative *In situ* hybridization (ISH)

For Rim1 in situ hybridisation, a 1124 bp Rim1 PCR product (covering nucleotides 376 to 1499 of the XM_129709 cDNA sequence) was inserted into a pCRII-TOPO cloning vector) as described in Lepagnol-Bestel et al., 2009). XhoI- or HindIII-linearised Rim1 inserts were used to generate antisense or sense [α35S]-rUTP (800 Ci/mmol, Amersham) labeled transcripts, using the P1460 riboprobe in vitro transcription systems (Promega), according to the manufacturer's instructions. Paraffin-embedded coronal 15 µm sections of P21 mouse brains,

including hippocampal structures, were selected for ISH. Sections were hybridised with radiolabelled RNA probe (diluted to 105 cpm/µl in 50% formamide hybridisation buffer) in 50% formamide at 50°C. Sections were successively washed in 50% formamide, 2 x SSC, 10 mM DTT at 65°C, and then in increasingly stringent SSC washing solution, with a final wash at 0.1 x SSC at 37°C. The regional distribution of radioactivity was analysed in the hippocampal region of wild-type and transgenic sections using a Micro Imager (Biospace Instruments) and the Betavision analysis program (Biospace Instruments).

Protein extraction and Western blot analysis.

HEK293 cells or mouse cortex (pool from three adult OF1 mice) were homogenized on ice in Tris-buffered saline (100 mM NaCl, 20 mM Tris-HCl, pH 7.4, 1% NP40, 1 x CIP). The homogenates were centrifuged at 13,000g for 10 min at 4°C and the supernatants were stored at -80 °C. Cell lysate protein concentration was determined using the BCA Protein assay kit (Thermofisher). For SDS-PAGE, 40µg of protein was diluted in Laemmli 1x (BioRad) with DTT and incubate for 5mn at 95°C. Proteic samples were loaded in each lane of a 4-15% precast polyacrylamide gel (BioRad) and ran in Mini-Protean at 200V in Tris/Glycine running buffer (BioRad). Following SDS-PAGE, proteins were semi-dry electroblotted onto nitrocellulose membranes using the Trans-Blot Turbo Transfer System (BioRad). Membranes were incubated for 1 h at room temperature in blocking solution (PBS 1x containing 5% non-fat dried milk, 0.05% Tween 20) and then for overnight at 4°C with the primary antibody. Primary antibodies used were as shown in Supplementary Table S3. Membranes were washed in PBS 1x containing 0.05% tween 20 and incubated for 1 h at room temperature with anti-mouse, anti-rabbit or anti-goat HRP-conjugated secondary antibody. Membranes were washed three times in PBS 1x containing 0.05% tween 20. Immune complexes were visualized using the Clarity Western ECL Substrate (BioRad). Chemiluminescence was detected using the ChemiDoc XRS Imaging System (BioRad). Primary antibodies used were as shown in Supplementary Table S3. As secondary antibodies, we used protein A or protein G IgG, HRP-conjugated whole antibody (1/5,000; Abcam ab7460 or ab7456 respectively).

Immunoprecipitation

1mg of protein extracts were incubated, after preclear with 50µL of dynabeads (Novex), 3h at 4°C under rotating with 10 µg of primary antibody (Supplementary Table S3; anti-mouse and anti-rabbit whole IgG (Millipore 12-371 and 12-370 respectively)). Add 50µL of protein A or protein G dynabeads and incubate 30mn at 4°C under rotating. Protein-antibody complexes were washed four times in 100 mM NaCl, 20 mM Tris-HCl, pH 7.4, 1% NP40 and analyzed by immunoblot.

Laser-assisted microdissection, Total RNA preparation and quantitative real-time PCR (Q-RT-PCR) analysis

Embryonic brain subregions were dissected as shown in Supplementary Figure. The left and right hippocampus was microdissected from genotyped P21 mouse brains using a laser-assisted capture microscope (Leica ASLMD instrument) with Leica polyethylene naphthalate membrane slides as described in Lepagnol-Bestel et al, 2009. RNA preparation and Q-RT-PCR are performed as described in Lepagnol-Bestel et al, 2009. Q-RT-PCR results are expressed in arbitrary unit.

Statistical analysis All data are shown as means+/-SEM. Statistics were performed using IgorPro (Wavemetrics), and statistical significance was determined by the Student's t test (two tailed distribution, paired) unless otherwise stated.

Reagents Stock solutions were prepared in water or DMSO, depending on the manufacturers' recommendation, and stored at -20°C. Upon experimentation, reagents were bath applied following dilution into ACSF (1/1000). D-APV and DCGIV were purchased from Tocris Bioscience. Salts for making cutting solution and ACSF were purchased from Sigma.

Bioinformatics evolutionary analysis

We performed 2 types of analysis. The first is based on extended haplotype homozygosity (EHH)[1], the second is the composite multiple signal method (CMS)[2,3].

Dataset We used 1'000G data4. For the EHH approach we used SNVs and INDELs data of Europeans individuals. We didn't use ancestrale status of variants for this analysis because this information was not available for all variants.

For the CMS method, we used 1'000G dataset of European, Asian and African population. We inferred ancestral status of SNPs using the snp138OrthoPt4Pa2Rm3 table from UCSC website. We used the chimpanzee allele as ancestral if it was available, if not, we used the orangutan allele, and after the macaque allele. If these three alleles were unavailable we discarded the SNPs. We discarded all SNPs with derived allele frequency below 5% and with null minor allele frequency in European population of 1'000G.

Long Haplotypes Method We used the R package rehh5 for this analysis. We calculated Integrated Haplotype Homozygosity (iHS) for all variants, standardized these scores within the chromosome according to frequency of minor allele and computed p-values (assuming iHS is normally distributed). We choose a cut-off of 3 and we obtained 211 variants from 120 016.

CMS method We performed a scan of chromosome 21(hg19) with the CMS method[2,3] using the CMS genome wide score (CMSGW) as described earlier in Grossman et al. (2012)[3].

Simulations We used the simulations described earlier in Grossman et al. (2010)[2]

We performed 1'000 simulations for neutral selection and 15 scenarii with 300 replicas each for selective sweep in European population with the cosi program6. We used different values for the time of the end of the selective sweep (200, 400, 800 generations) and for the final frequency of the selected allele (0.2, 0.4, 0.6, 0.8, 1). Simulated regions were 1Mbp length and the selected alleles were in the middle of these regions as described previously.

CMS We used the CMSGW as described previously with minor changes:

- for the XPEHH-test. We used the XPEHH-test versus the 2 populations (AFR and ASN, 2 distributions) instead of taking the maximum value of the test according to 2 other populations.
- We used nucleotidic distance instead of genetic distance for the XPEHH-test and iHS test.

We computed CMSGW score of SNPs for which we had complete statistics (no infinite values, or missing data). This dataset represents 91639 SNPs on chr21. We used a cut-off on log10(score) of 2 corresponding approximatively of top 1% SNPs (see Supplementary Figure). We identified 100kb regions in which 30 % of SNPs were in our top 1% (see Figure).

Venn Diagram Chr21 value indicates the number of coding genes carried by this chromosome. Long haplotypes value indicates the number of coding genes intersected by significant variants. CMS value indicates the number of coding genes intersected by significant SNPs with this method.

ACKNOWLEDGMENTS

We would like to acknowledge the funding support from the European Union's Seventh Framework Programme for research, technological development and demonstration AgedBrainSYSBIO under grant agreement No. 305299 (to M.S.) and Fondation Lejeune. This work was also partly funded by INSERM, European JPND (TransPathND) and CNES (to M.S.).

REFERENCES

1. S. E. Antonarakis, Down syndrome and the complexity of genome dosage imbalance. *Nat. Rev. Genet.* **18**, 147–163 (2017).

2. S. E. Antonarakis, R. Lyle, E. T. Dermitzakis, A. Reymond, S. Deutsch, Chromosome 21 and down syndrome: from genomics to pathophysiology. *Nat. Rev. Genet.* **5**, 725–738 (2004).

3. C. Ballard, W. Mobley, J. Hardy, G. Williams, A. Corbett, Dementia in Down's syndrome. *Lancet Neurol* **15**, 622–636 (2016).

4. M. Dierssen, Down syndrome: the brain in trisomic mode. *Nature Reviews Neuroscience* **13**, 844–858 (2012).

5. F. K. Wiseman, *et al.*, A genetic cause of Alzheimer disease: mechanistic insights from Down syndrome. *Nat. Rev. Neurosci.* **16**, 564–574 (2015).

6. F. Guedj, *et al.*, DYRK1A: a master regulatory protein controlling brain growth. *Neurobiol. Dis.* **46**, 190–203 (2012).

7. T. Yu, *et al.*, A mouse model of Down syndrome trisomic for all human chromosome 21 syntenic regions. *Hum. Mol. Genet.* **19**, 2780–2791 (2010).

8. K.-J. Ahn, *et al.*, DYRK1A BAC transgenic mice show altered synaptic plasticity with learning and memory defects. *Neurobiol. Dis.* **22**, 463–472 (2006).

9. A. Thomazeau, *et al.*, Prefrontal deficits in a murine model overexpressing the down syndrome candidate gene dyrk1a. *J. Neurosci.* **34**, 1138–1147 (2014).

10. D. J. Smith, *et al.*, Functional screening of 2 Mb of human chromosome 21q22.2 in transgenic mice implicates minibrain in learning defects associated with Down syndrome. *Nature Genetics* **16**, 28–36 (1997).

11. A.-M. Lepagnol-Bestel, *et al.*, DYRK1A interacts with the REST/NRSF-SWI/SNF chromatin remodelling complex to deregulate gene clusters involved in the neuronal phenotypic traits of Down syndrome. *Hum. Mol. Genet.* **18**, 1405–1414 (2009).

12. Y. Loe-Mie, *et al.*, SMARCA2 and other genome-wide supported schizophrenia-associated genes: regulation by REST/NRSF, network organization and primate-specific evolution. *Hum. Mol. Genet.* **19**, 2841–2857 (2010).

13. A. M. Kleschevnikov, *et al.*, Deficits in cognition and synaptic plasticity in a mouse model of Down syndrome ameliorated by GABAB receptor antagonists. *J. Neurosci.* **32**, 9217–9227 (2012).

14. M. Raveau, *et al.*, Alterations of in vivo CA1 network activity in Dp(16)1Yey Down syndrome model mice. *Elife* **7** (2018).

15. E. J. Rossin, *et al.*, Proteins encoded in genomic regions associated with immune-mediated disease physically interact and suggest underlying biology. *PLoS Genet.* **7**, e1001273 (2011).

16. Y. Liao, J. Wang, E. J. Jaehnig, Z. Shi, B. Zhang, WebGestalt 2019: gene set analysis toolkit with revamped UIs and APIs. *Nucleic Acids Res.* **47**, W199–W205 (2019).

17. E. Fernández, *et al.*, Arc Requires PSD95 for Assembly into Postsynaptic Complexes Involved with Neural Dysfunction and Intelligence. *Cell Rep* **21**, 679–691 (2017).

18. E. Formstecher, *et al.*, Protein interaction mapping: a Drosophila case study. *Genome Res.* **15**, 376–384 (2005).

19. Deciphering Developmental Disorders Study, Large-scale discovery of novel genetic causes of developmental disorders. *Nature* **519**, 223–228 (2015).

20. C. Gilissen, *et al.*, Genome sequencing identifies major causes of severe intellectual disability. *Nature* **511**, 344–347 (2014).

21. O. Söderberg, *et al.*, Direct observation of individual endogenous protein complexes in situ by proximity ligation. *Nat. Methods* **3**, 995–1000 (2006).

22. K. Takamatsu, *et al.*, Identification of two novel primate-specific genes in DSCR. *DNA Res.* **9**, 89–97 (2002).

23. J. C. Lambert, *et al.*, Meta-analysis of 74,046 individuals identifies 11 new susceptibility loci for Alzheimer's disease. *Nat. Genet.* **45**, 1452–1458 (2013).

24. B. W. Kunkle, *et al.*, Genetic meta-analysis of diagnosed Alzheimer's disease identifies new risk loci and implicates Aβ, tau, immunity and lipid processing. *Nat. Genet.* **51**, 414–430 (2019).

25. R. C. Wilson, J. A. Doudna, Molecular mechanisms of RNA interference. *Annu Rev Biophys* **42**, 217–239 (2013).

26. K. Fénelon, *et al.*, Deficiency of Dgcr8, a gene disrupted by the 22q11.2 microdeletion, results in altered short-term plasticity in the prefrontal cortex. *Proc. Natl. Acad. Sci. U.S.A.* **108**, 4447–4452 (2011).

27. S. S. Hébert, B. De Strooper, Alterations of the microRNA network cause neurodegenerative disease. *Trends Neurosci.* **32**, 199–206 (2009).

28. J. Li, *et al.*, Long-term potentiation modulates synaptic phosphorylation networks and reshapes the structure of the postsynaptic interactome. *Sci Signal* **9**, rs8 (2016).

29. J. Li, *et al.*, Spatiotemporal profile of postsynaptic interactomes integrates components of complex brain disorders. *Nat. Neurosci.* **20**, 1150–1161 (2017).

30. J. Lerma, J. M. Marques, Kainate receptors in health and disease. *Neuron* **80**, 292–311 (2013).

31. A. F. T. Arnsten, M. J. Wang, C. D. Paspalas, Neuromodulation of thought: flexibilities and vulnerabilities in prefrontal cortical network synapses. *Neuron* **76**, 223–239 (2012).

32. T. Tada, *et al.*, Role of Septin cytoskeleton in spine morphogenesis and dendrite development in neurons. *Curr. Biol.* **17**, 1752–1758 (2007).

33. P. Penzes, K. A. Jones, Dendritic spine dynamics--a key role for kalirin-7. *Trends Neurosci.* **31**, 419–427 (2008).

34. D. D. Kiraly, F. Lemtiri-Chlieh, E. S. Levine, R. E. Mains, B. A. Eipper, Kalirin binds the NR2B subunit of the NMDA receptor, altering its synaptic localization and function. *J. Neurosci.* **31**, 12554–12565 (2011).

35. Y. Oku, R. L. Huganir, AGAP3 and Arf6 regulate trafficking of AMPA receptors and synaptic plasticity. *J. Neurosci.* **33**, 12586–12598 (2013).

36. E. Korkotian, M. Frotscher, M. Segal, Synaptopodin regulates spine plasticity: mediation by calcium stores. *J. Neurosci.* **34**, 11641–11651 (2014).

37. J. M. Frangiskakis, *et al.*, LIM-kinase1 hemizygosity implicated in impaired visuospatial constructive cognition. *Cell* **86**, 59–69 (1996).

38. P. Penzes, I. Rafalovich, Regulation of the actin cytoskeleton in dendritic spines. *Adv. Exp. Med. Biol.* **970**, 81–95 (2012).

39. S. Rao, Y. Kay, B. E. Herring, Tiam1 is Critical for Glutamatergic Synapse Structure and Function in the Hippocampus. *J. Neurosci.* **39**, 9306–9315 (2019).

40. R. Daudin, *et al.*, BIN1 genetic risk factor for Alzheimer is sufficient to induce early structural tract alterations in entorhinal cortex-dentate gyrus pathway and related hippocampal multi-scale impairments. *bioRxiv*, 437228 (2018).

41. B. Schürmann, *et al.*, A novel role for the late-onset Alzheimer's disease (LOAD)-associated protein Bin1 in regulating postsynaptic trafficking and glutamatergic signaling. *Mol. Psychiatry* (2019) https:/doi.org/10.1038/s41380-019-0407-3.

42. C. T. Drake, S. B. Bausch, T. A. Milner, C. Chavkin, GIRK1 immunoreactivity is present predominantly in dendrites, dendritic spines, and somata in the CA1 region of the hippocampus. *Proc. Natl. Acad. Sci. U.S.A.* **94**, 1007–1012 (1997).

43. R. Luján, J. Maylie, J. P. Adelman, New sites of action for GIRK and SK channels. *Nat. Rev. Neurosci.* **10**, 475–480 (2009).

44. A. Cooper, *et al.*, Trisomy of the G protein-coupled K+ channel gene, Kcnj6, affects reward mechanisms, cognitive functions, and synaptic plasticity in mice. *Proc. Natl. Acad. Sci. U.S.A.* **109**, 2642–2647 (2012).

45. T. C. Südhof, J. E. Rothman, Membrane fusion: grappling with SNARE and SM proteins. *Science* **323**, 474–477 (2009).

46. S. Jurado, *et al.*, LTP requires a unique postsynaptic SNARE fusion machinery. *Neuron* **77**, 542–558 (2013).

47. R. Tomasoni, *et al.*, SNAP-25 regulates spine formation through postsynaptic binding to p140Cap. *Nat Commun* **4**, 2136 (2013).

48. E. Kim, *et al.*, GKAP, a novel synaptic protein that interacts with the guanylate kinase-like domain of the PSD-95/SAP90 family of channel clustering molecules. *J. Cell Biol.* **136**, 669–678 (1997).

49. A. S. Sengar, *et al.*, Vertebrate intersectin1 is repurposed to facilitate cortical midline connectivity and higher order cognition. *J. Neurosci.* **33**, 4055–4065 (2013).

50. B. Jakob, *et al.*, Intersectin 1 is a component of the Reelin pathway to regulate neuronal migration and synaptic plasticity in the hippocampus. *Proc. Natl. Acad. Sci. U.S.A.* **114**, 5533–5538 (2017).

51. D. T. S. Pak, M. Sheng, Targeted protein degradation and synapse remodeling by an inducible protein kinase. *Science* **302**, 1368–1373 (2003).

52. D. T. Pak, S. Yang, S. Rudolph-Correia, E. Kim, M. Sheng, Regulation of dendritic spine morphology by SPAR, a PSD-95-associated RapGAP. *Neuron* **31**, 289–303 (2001).

53. K. R. Maynard, E. Stein, DSCAM contributes to dendrite arborization and spine formation in the developing cerebral cortex. *J. Neurosci.* **32**, 16637–16650 (2012).

54. E. Kim, M. Sheng, PDZ domain proteins of synapses. *Nat. Rev. Neurosci.* **5**, 771–781 (2004).

55. M. Sheng, E. Kim, The postsynaptic organization of synapses. *Cold Spring Harb Perspect Biol* **3** (2011).

56. J. Nithianantharajah, *et al.*, Synaptic scaffold evolution generated components of vertebrate cognitive complexity. *Nat. Neurosci.* **16**, 16–24 (2013).

57. C.-L. Tao, *et al.*, Differentiation and Characterization of Excitatory and Inhibitory Synapses by Cryo-electron Tomography and Correlative Microscopy. *J. Neurosci.* **38**, 1493–1510 (2018).

58. S. J. Sanders, *et al.*, Insights into Autism Spectrum Disorder Genomic Architecture and Biology from 71 Risk Loci. *Neuron* **87**, 1215–1233 (2015).

59. A. J. Willsey, *et al.*, The Psychiatric Cell Map Initiative: A Convergent Systems Biological Approach to Illuminating Key Molecular Pathways in Neuropsychiatric Disorders. *Cell* **174**, 505–520 (2018).

60. C. M. Karch, C. Cruchaga, A. M. Goate, Alzheimer's disease genetics: from the bench to the clinic. *Neuron* **83**, 11–26 (2014).

61. S. G. N. Grant, The Synaptomic Theory of Behavior and Brain Disease. *Cold Spring Harb. Symp. Quant. Biol.* **83**, 45–56 (2018).

62. F. Koopmans, *et al.*, SynGO: An Evidence-Based, Expert-Curated Knowledge Base for the Synapse. *Neuron* **103**, 217-234.e4 (2019).

63. F. K. Wiseman, *et al.*, A genetic cause of Alzheimer disease: mechanistic insights from Down syndrome. *Nat. Rev. Neurosci.* **16**, 564–574 (2015).

64. A. Nott, *et al.*, Brain cell type-specific enhancer-promoter interactome maps and disease-risk association. *Science* **366**, 1134–1139 (2019).

65. M. Hruska, N. Henderson, S. J. Le Marchand, H. Jafri, M. B. Dalva, Synaptic nanomodules underlie the organization and plasticity of spine synapses. *Nat. Neurosci.* **21**, 671–682 (2018).

66. A.-H. Tang, *et al.*, A trans-synaptic nanocolumn aligns neurotransmitter release to receptors. *Nature* **536**, 210–214 (2016).

67. F. Laumonnier, *et al.*, X-linked mental retardation and autism are associated with a mutation in the NLGN4 gene, a member of the neuroligin family. *Am. J. Hum. Genet.* **74**, 552–557 (2004).

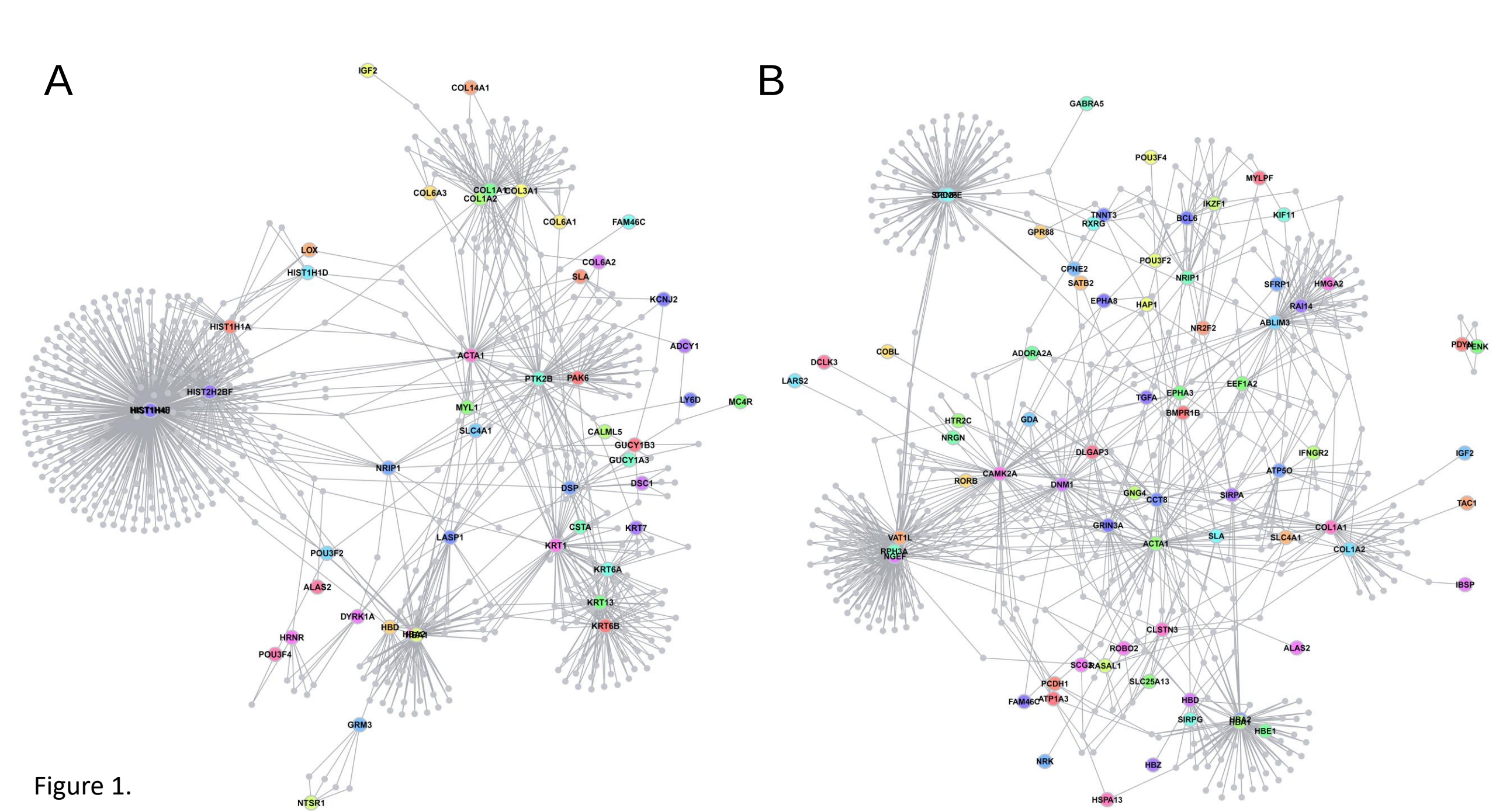
A
IGF2
COL14A1
COL6A3
COL1A1
COL3A1
COL1A2
COL6A1
FAM46C
LOX
HIST1H1D
COL6A2
SLA
KCNJ2
HIST1H1A
ADCY1
ACTA1
PTK2B
PAK6
HIST2H2BF
LY6D
MC4R
MYL1
SLC4A1
CALML5
GUCY1B3
GUCY1A3
NRIP1
DSP
DSC1
CSTA
KRT7
LASP1
KRT1
POU3F2
KRT6A
ALAS2
KRT13
DYRK1A
HBD
KRT6B
HRNR
POU3F4
GRM3
NTSR1
B
GABRA5
POU3F4
MYLPF
IKZF1
TNNT3
RXRG
BCL6
KIF11
GPR88
CPNE2
POU3F2
NRIP1
SATB2
SFRP1
HMGA2
EPHA8
HAP1
RAI14
NR2F2
ABLIM3
PDYN
ENK
COBL
ADORA2A
DCLK3
LARS2
EEF1A2
TGFA
EPHA3
BMPR1B
HTR2C
GDA
NRGN
DLGAP3
IFNGR2
IGF2
CAMK2A
ATP5O
RORB
DNM1
GNG4
CCT8
SIRPA
TAC1
GRIN3A
COL1A1
VAT1L
ACTA1
SLA
SLC4A1
COL1A2
IBSP
CLSTN3
ROBO2
ALAS2
PCDH1
SLC25A13
FAM46C
ATP1A3
HBD
SIRPG
HBE1
NRK
HBZ
HSPA13

Figure 1.

Figure 1. Protein-Protein Interaction Network generated from proteins encoded by deregulated genes identified in E17 hippocampus of 189N3 and Dp(16)1Yey transgenic mouse models, respectively.

We performed RNA sequencing on embryonic E17 hippocampi of these two DS models. We identified 84 deregulated genes in 189N3 (**Supplementary Table S1**) and 142 deregulated genes in Dp(16)1Yey/+ (**Supplementary Table S2**) compared to their littermate controls. They were included as an input to DAPPLE. Disease Association Protein-Protein Link Evaluator (DAPPLE), which uses high-confidence pairwise protein interactions and tissue-specific expression data to reconstruct a PPI network (Rossin et al., 2012). The network is conservative, requiring that interacting proteins be known to be coexpressed in a given tissue. Proteins encoded by deregulated genes are represented as nodes connected by an edge if there is in vitro evidence for high-confidence interaction.

A: for 189N3 mice, we found an enrichment in Gene ontology (GO) Process analyses of differentially expressed genes revealed a deregulation of chromatin proteins for 189N3 mice with: GO:0006334~nucleosome assembly (P value=1.17 e^{-08}). The DAPPLE network based on the analysis of 75 genes is statistically significant for direct and indirect connectivity more than would be expected by chance .

For direct connectivity: Direct edges Count 26; expected 5.5; permuted 9.99 x 10^{-4}; Seed Direct Degrees Mean 2.26: expected 1.27; permuted p=9.99 x 10^{-3}.

For indirect connectivity, Seed Indirect Degrees Mean 52.54; expected 29.43; permuted 9.99 x 10^{-4}; CI Degrees Mean 2.51; expected 2.28; permuted p=2.99 x 10^{-3}.

B: for Dp(16)1Yey/+, we found a deregulation of proteins involved in synaptic function:GO:0007268~chemical synaptic transmission (Pvalue= 6.87e-^{09}). The network based on the analysis of 131 genes is statistically significant for direct connectivity more than would be expected by chance (Direct edges count, 16; expected 7.933; permuted p=1.09 x 10^{-2}). genes

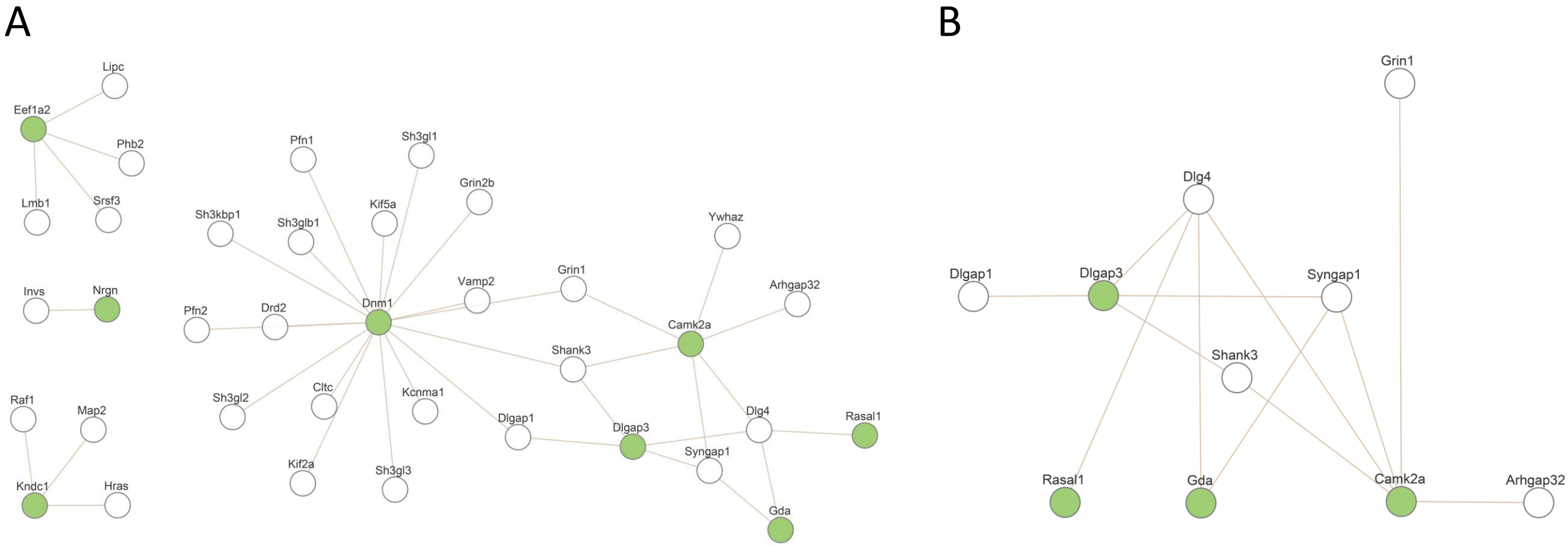
A
Lipc
Eef1a2
Phb2
Lmb1
Srsf3
Invs
Nrgn
Raf1
Map2
Kndc1
Hras
Pfn1
Sh3gl1
Grin2b
Sh3kbp1
Sh3glb1
Kif5a
Ywhaz
Vamp2
Grin1
Arhgap32
Pfn2
Drd2
Dnm1
Camk2a
Shank3
Sh3gl2
Cltc
Kcnma1
Dlgap1
Dlgap3
Dlg4
Rasal1
Syngap1
Kif2a
Sh3gl3
Gda
B
Grin1
Dlg4
Dlgap1
Dlgap3
Syngap1
Shank3
Rasal1
Gda
Camk2a
Arhgap32

Figure 2.

Figure 2. Products of deregulated genes in Dp(16)1Yey/+ are enriched in proteins linked to glutamate receptor signaling pathway and in proteins involved in an ARC-PSD95 complex linked to ID and intelligence.

We found 142 deregulated genes in Dp(16)1Yey/+ with 77 upregulated. Using Webgestalt suite, we identified two significant networks (A) and (B).**A**: a network that includes 8 genes from the 70 upregulated list with an enrichment in GO Biological Process: chemical synaptic transmission (p=220446e-16). **B**: a network that includes 4 genes from the 77 upregulated list with an enrichment in GO Biological Process: Biological Process: glutamate receptor signaling pathway (p=220446e-16). Note that the 3 genes (Camk2a, Gda, Dlgap3) are part of a protein network of ARC-dependent DLG4 interactors that include 20 proteins (Hernandez et al., 2018), indicating an over enrichment of 43.85 fold compared to expectations (hypergeometric p-value = 4.20 e-05).
[Parameters: 3, 20, 77, 22,508 number of mouse genes from Mouse Ensembl (GRCm38.p6)].

Figure 3.

A Chr21 baits/novel

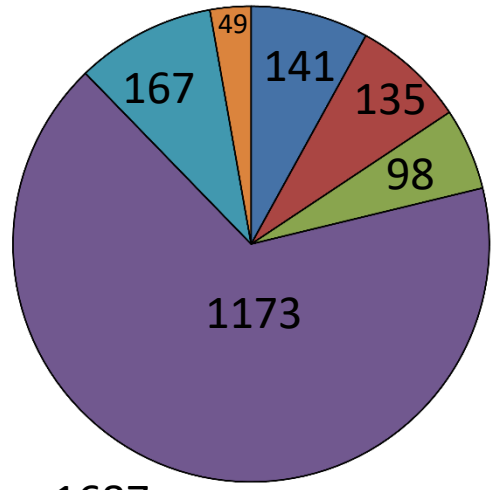

n=1687

B Chr21 baits/already described

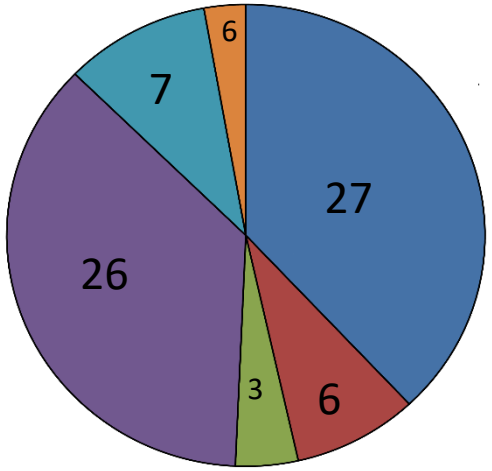

n=76

S2 -1200
S10- 450
S11- 620

a
b

C Rebounds/novel

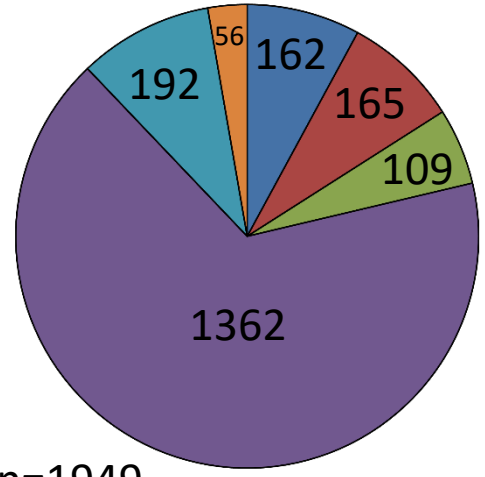

n=1949

D Rebounds/already described

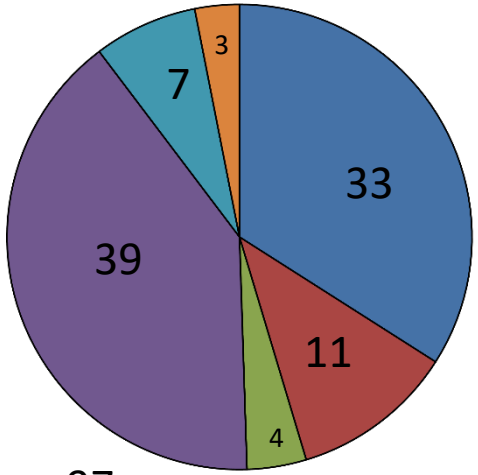

n=97

c
d
e
f

E

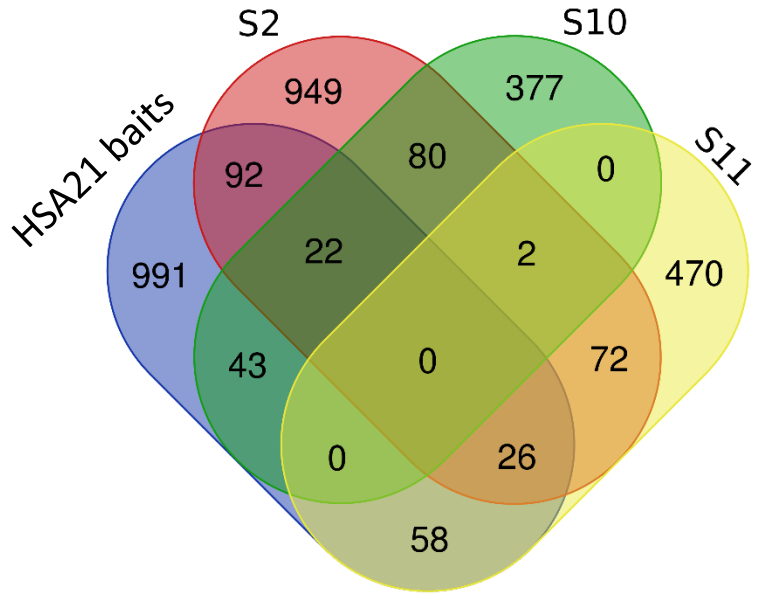

F

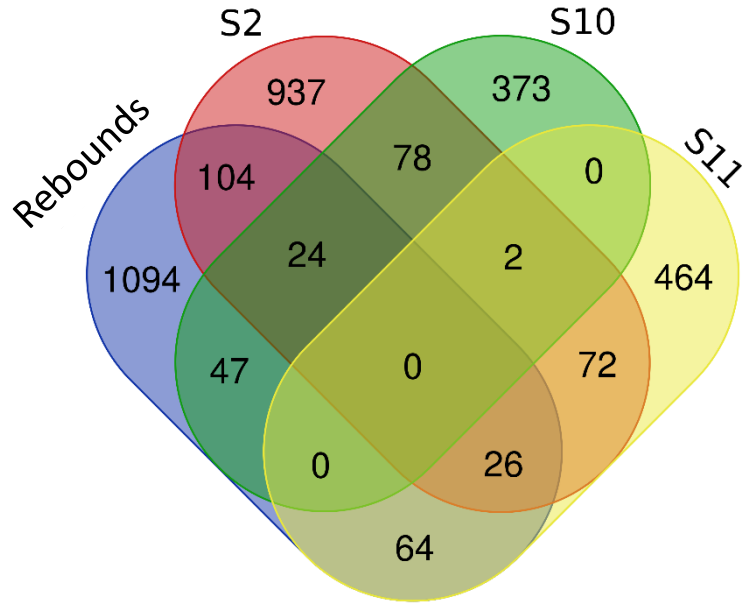

Fig.3 high-throughput Y2H identifies 3636 novel direct interactions with their enrichment in proteins involved in Intellectual Disabilities

72 screens with HSA21 protein as baits and 82 screens against their direct interactors (rebounds) have been performed using a human brain library. 1687 and 1949 novel direct interactions have been identified. These interactions were ranked by category (a to f), using a Predicted Biological Score (PBS) (Formstecher et al., 2005).
Analysis of direct interactors from 72 HSA21 baits screens (**A-C**).1687 novel interactions were identified (**A**) and 76 already known (Biogrid) interactions confirmed (**B**).
Analysis of direct interactors from 82 rebound screens (**D-F**). 1949 novel interactions were identified (**D**) and 97 already known (Biogrid) interactions confirmed (**E**).
We compared these direct interactors with three lists of genes involved in Intellectual Disability (Gilissen et al. Nature, 2014; Deciphering Developmental Disorders Study, 2015). Both HSA21 direct interactors (**C**) and rebound direct interactors (**F**) are enriched in ID proteins (see text) suggesting that these two types of interactors are part of a large ID network.

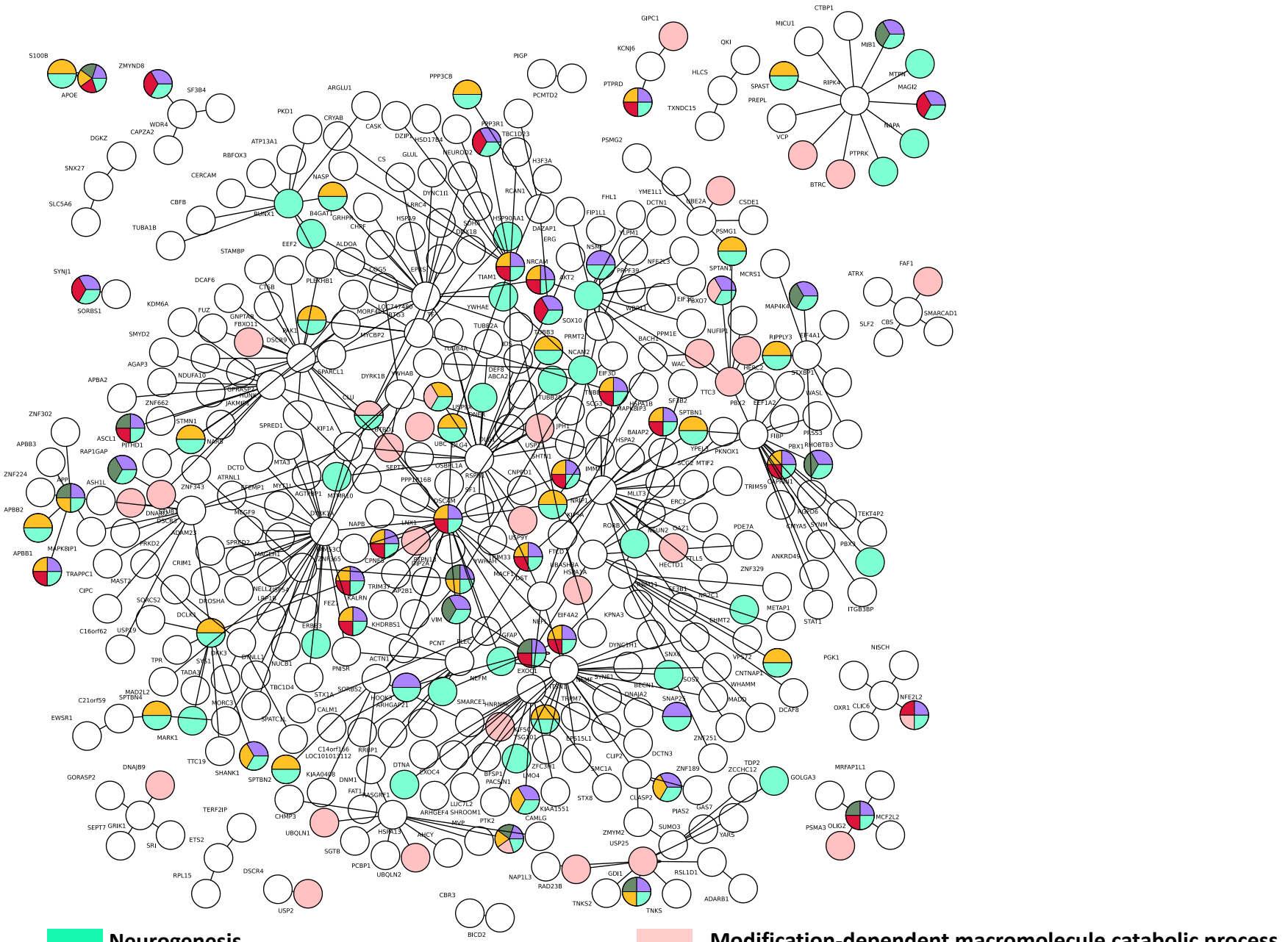
Neurogenesis
Neuron projection morphogenesis
Regulation of neurogenesis
Modification-dependent macromolecule catabolic process
Positive regulation of nervous system development
Negative regulation of neuron differentiation

Figure 4.

Figure 4: Biological processes network interactions from Yeast two-hybrid protein-protein interaction data.
A biological processes analysis using GO DAVID was realized (see methods). The colored nodes correspond to the most significative results: GO:0022008~Neurogenesis; GO:0048812~Neuron projection morphogenesis; GO:0050767~Regulation of neurogenesis; GO:0043632~Modification-dependent macromolecule catabolic process; GO:0051962~Positive regulation of nervous system development; GO:0045665~Negative regulation of neuron differentiation with *p*-value 3.06e-17, 2.91e-13, 2.66e-06, 6.46e-05, 6.29e-06,1.55e-07, respectively). A color correspond to a cluster of several biological processes. The multi-colored nodes correspond to genes presents in different annotation clusters.

Figure 5

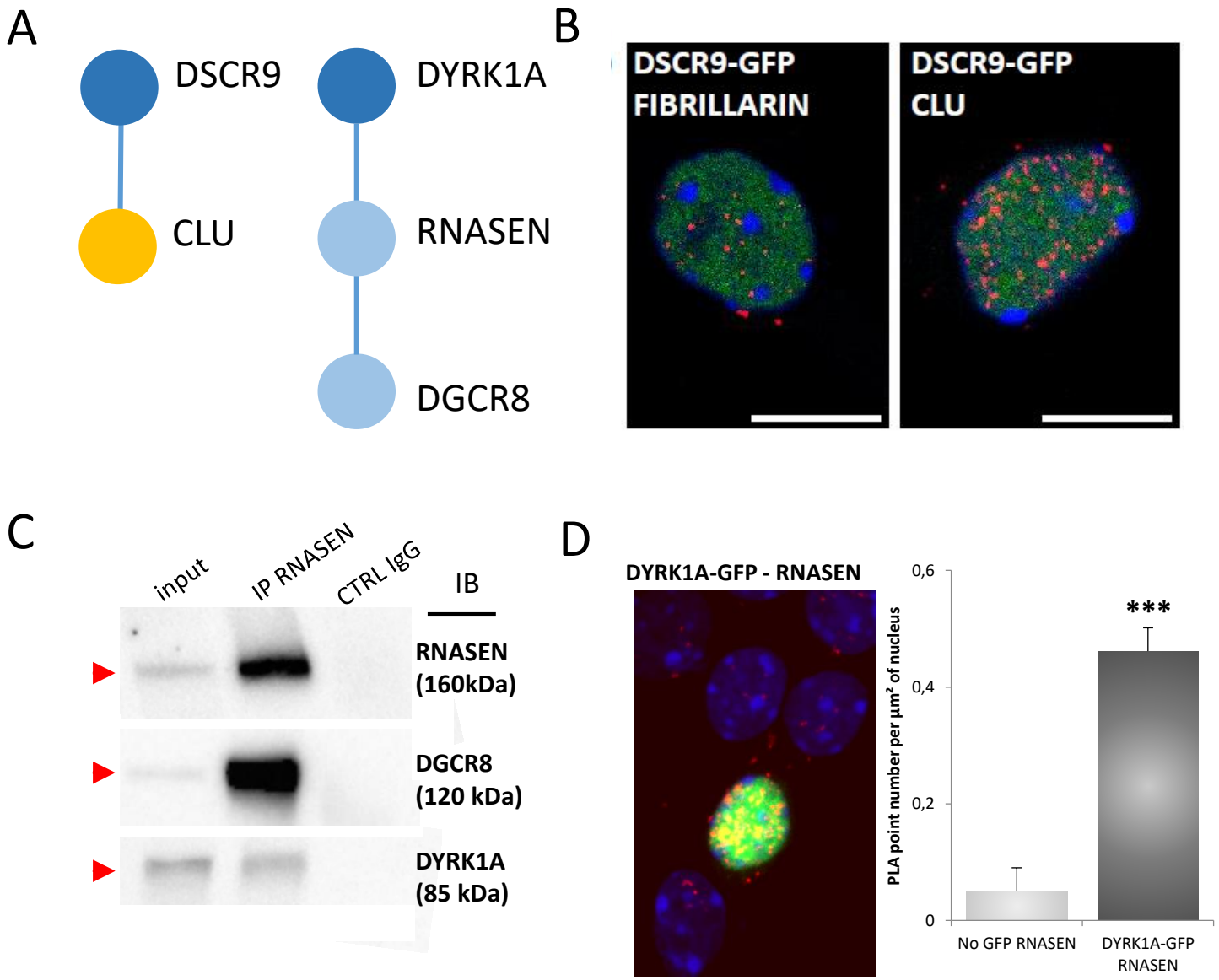
A
DSCR9
CLU
DYRK1A
RNASEN
DGCR8
B
DSCR9-GFP
FIBRILLARIN
DSCR9-GFP
CLU
C
input
IP RNASEN
CTRL IgG
IB
RNASEN
(160kDa)
DGCR8
(120 kDa)
DYRK1A
(85 kDa)
D
DYRK1A-GFP - RNASEN
PLA point number per µm² of nucleus
0,6
0,4
0,2
0
***
No GFP RNASEN
DYRK1A-GFP
RNASEN

Figure 5. Interactions of HSA21 proteins with proteins involved in LOAD, Intellectual Disability and neuropsychiatric diseases

(**A**). Schematic representation of protein-protein interactions identified by yeast-two-hybrid using a human brain library. Dark blue circles indicate HSA21 encoded proteins; orange circle indicates a LOAD-related protein. (**B)**. *In situ* PLA on primary cortical neurons transfected at DIC5 and fixed 48 hours later at DIC7 (red fluorescence) using anti-GFP and anti-Clu antibodies. PLA using anti-GFP and anti-Fibrillarin antibodies were performed as a negative control. Green fluorescent protein was visualized on green channel and nuclear bodies were labelled using Topro3 (blue fluorescence). (**C**) and (**D**): DYRK1A interaction with RNASEN. (**C**): EK293 cells were immunoprecipitated (IP) using anti-RNASEN antibody and anti-IgG antibody as a negative control. The input and precipitated fractions were then resolved by sodium dodecyl sulphate–polyacrylamide gel electrophoresis (SDS–PAGE) and analyzed by western blot using anti-Rnasen, anti-Dgcr8 and anti-Dyrk1a antibodies. The arrows indicate protein bands at the expected size. Note that no cross-reaction was found with the IgGs. (**D**): *In situ* proximity ligation assays PLA on primary cortical neurons transfected at DIC5 with Dyrk1a-GFP construct (green fluorescence) and fixed at DIC7, using anti-GFP and anti-Rnasen antibodies (red fluorescence). Non-transfected neurons were used as a negative control. Nuclei were labelled using Topro3 staining (blue fluorescence). Mean interaction point numbers were calculated in nuclear body of at least 25 transfected cortical neurons. *** $p<0.0005$.

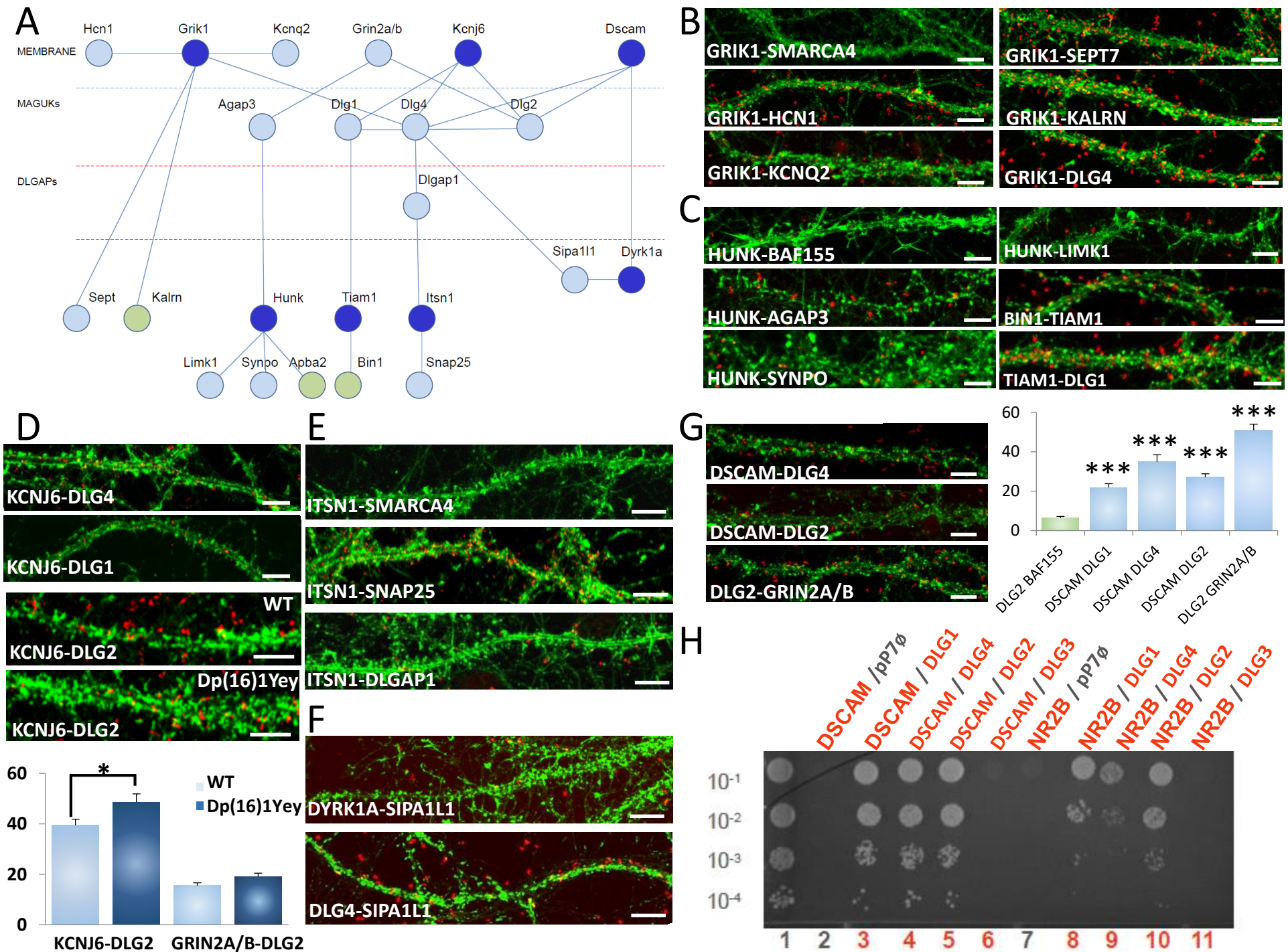
A
MEMBRANE
MAGUKs
DLGAPs
Hcn1
Grik1
Kcnq2
Grin2a/b
Kcnj6
Dscam
Agap3
Dlg1
Dlg4
Dlg2
Dlgap1
Sipa1l1
Dyrk1a
Sept
Kalrn
Hunk
Tiam1
Itsn1
Limk1
Synpo
Apba2
Bin1
Snap25
B
GRIK1-SMARCA4
GRIK1-SEPT7
GRIK1-HCN1
GRIK1-KALRN
GRIK1-KCNQ2
GRIK1-DLG4
C
HUNK-BAF155
HUNK-LIMK1
HUNK-AGAP3
BIN1-TIAM1
HUNK-SYNPO
TIAM1-DLG1
D
KCNJ6-DLG4
KCNJ6-DLG1
WT
KCNJ6-DLG2
Dp(16)1Yey
KCNJ6-DLG2
60
40
20
0
*
WT
Dp(16)1Yey
KCNJ6-DLG2
GRIN2A/B-DLG2
E
ITSN1-SMARCA4
ITSN1-SNAP25
ITSN1-DLGAP1
F
DYRK1A-SIPA1L1
DLG4-SIPA1L1
G
DSCAM-DLG4
DSCAM-DLG2
DLG2-GRIN2A/B
60
40
20
0
***
***
***
***
DLG2 BAF155
DSCAM DLG1
DSCAM DLG4
DSCAM DLG2
DLG2 GRIN2A/B
H
DSCAM /pP7ϕ
DSCAM / DLG1
DSCAM / DLG4
DSCAM / DLG2
DSCAM / DLG3
NR2B / pP7ϕ
NR2B / DLG1
NR2B / DLG4
NR2B / DLG2
NR2B / DLG3
10-1
10-2
10-3
10-4
1 2 3 4 5 6 7 8 9 10 11

Figure 6. Chr21-encoded proteins have direct interactors in dendritic spine PSD

a. Schematic representation of synaptic protein-protein interactions performed by yeast-two-hybrid with the three layers of dendritic spine PSDs. Chr21-encoded proteins and LOAD-related proteins are indicated by dark blue and green circles respectively. b-g. *In situ* proximity ligation assays (PLA) on primary cortical neurons fixed at DIC21 (red fluorescence) using anti-Grik1 and anti-Hcn1, anti-Kcnq2, anti-Sept7,anti-Kalrn or anti-Dlg4 antibodies (b), anti-Hunk and anti-Agap3, anti-Synpo and anti-Limk1 and also anti-Tiam1 and anti-Bin1 or anti-Dlg1 (c), anti-Kcnj6 and anti-Dlg4 or anti-Dlg2 antibodies (d), anti-Itsn1 and anti-Snap25 or anti-Dlgap1 (e), anti-Sipa1l1 and anti-Dyrk1a or anti-Dlg4 antibodies (f), anti-Dscam and anti-Dlg2 or anti-Dlg4 or anti-Grin2a/b antibodies (g). PLA using anti-Grik1 and anti-Dlg4 (b), anti-Hunk and anti-Synpo (c), anti-Kcnj6 and anti-Dlg1 (d), anti-Itsn1 and anti-Snap25 (e), anti-Sipa1l1 and anti-Dlg4 (f) and anti-Dlg2 and anti-Grin2ab (g) were performed as positive controls. PLA using either anti-Smarca4 or anti-Baf155 antibodies were performed as negative control. Dendritic network and dendritic spines were labelled using phalloidin staining (green fluorescence). Mean interaction point numbers were calculated in dendrites of 25 to 30 cortical neurons at DIC21. Please see Supplementary Figure for negative controls. d. *In situ* PLA on transgenic Dp(16)1Yey and WT primary cortical neurons fixed at DIC21 (red fluorescence) using anti-Dlg2 and anti-Kcnj6 or anti-Grin2ab antibodies. Dendritic network and dendritic spines were labelled using phalloidin staining (green fluorescence). Mean interaction point numbers were calculated in dendrites of at least 26 cortical neurons at DIC21 (from 3 different embryos per genotype). * $p < 0.05$ Scale bars=10µm. h. Yeast two-hybrid one-by-one assays revealed DSCAM and NR2B as interactors of some of DLGs. Lane 1 is the positive control. Lanes 2 and 7 are the negative controls (pP7-DSCAM or pP7-NR2B vector with empty pP7 vector). Lanes 3 to 6 and 8 to 11 are the DSCAM and NR2B interactions respectively.

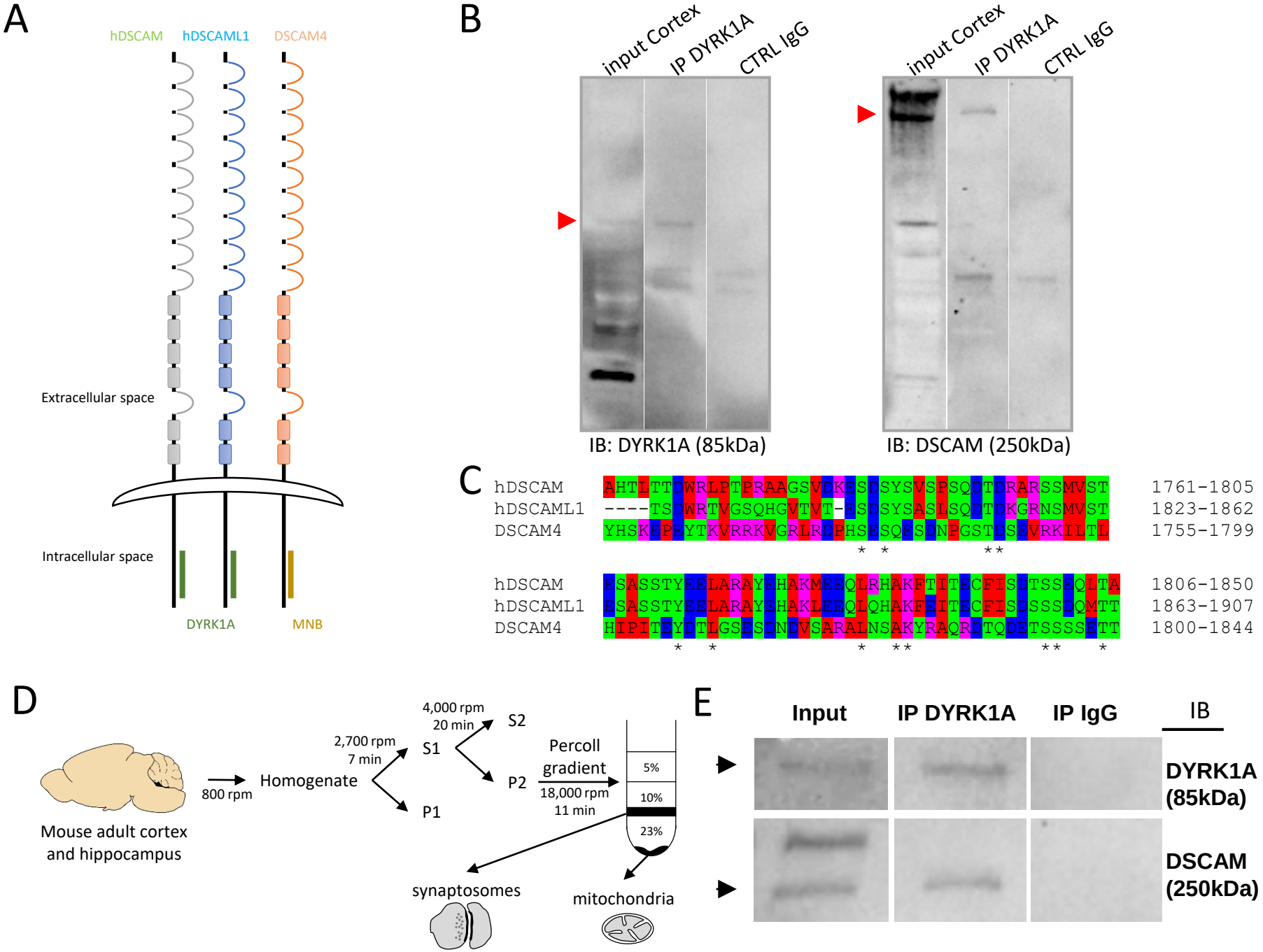
A
hDSCAM
hDSCAML1
DSCAM4
Extracellular space
Intracellular space
DYRK1A
MNB
B
input Cortex
IP DYRK1A
CTRL IgG
IB: DYRK1A (85kDa)
input Cortex
IP DYRK1A
CTRL IgG
IB: DSCAM (250kDa)
C
hDSCAM AHTLTTDWRLPTPRAAGSVDKESDSYSVSPSQDTDRARSSMVST 1761-1805
hDSCAML1 ----TSDWRTVGSQHGVTVT-ESDSYSASLSQDTDKGRNSMVST 1823-1862
DSCAM4 YHSKEPEYTKVRRKVGRLRDPHSPSQESDNPGSTDSEVRKILTL 1755-1799
hDSCAM ESASSTYEELARAYEHAKMEEQLRHAKFTITECFISDTSSMQLTA 1806-1850
hDSCAML1 ESASSTYEELARAYEHAKLEEQLQHAKFEITECFISDSSSDQMTT 1863-1907
DSCAM4 HIPITHYDTLGSESDNDVSARALNSAKYRAQRDTQDETSSSSETT 1800-1844
D
Mouse adult cortex and hippocampus
800 rpm
Homogenate
2,700 rpm 7 min
S1
P1
4,000 rpm 20 min
S2
P2
Percoll gradient
18,000 rpm 11 min
5%
10%
23%
synaptosomes
mitochondria
E
Input
IP DYRK1A
IP IgG
IB
DYRK1A (85kDa)
DSCAM (250kDa)

Figure 7. Conservation of DSCAM-DYRK1A interaction through evolution

A. Schematic representation of DSCAM and DYRK1A protein family interaction. Human DSCAM (hDSCAM in green), human DSCAML1 (hDSCAML1 in blue) and its drosophila orthologus (dDSCAM4 in red) share the same conserved proteic domain interacting with human DYRK1A (hDYRK1A) or its drosophila orthologus (MNB) respectively. **B**. Adult mouse cortical protein extract were immunoprecipitated (IP) using anti-Dyrk1a antibody and anti-IgG antiboby as a negative control. The input and precipitated fractions were then resolved by sodium dodecyl sulphate–polyacrylamide gel electrophoresis (SDS–PAGE) and analyzed by western blot using anti-Dyrk1a and anti-Dscam antibody. Red arrows indicate protein bands at the expected size. Note that no cross-reaction was found with the IgGs. **C**. Amino acid alignment of the DSCAM domain that interacts with DYRK1A and Minibrain. This alignment was performed with ClustalW 2.1 software. **D**. Schematic representation of synaptosome enrichment protocol. **E**. Adult mouse cortical protein extracts were immunoprecipitated (IP) using anti-Dyrk1a antibody and anti-IgG antibody as a negative control. The input and precipitated fractions were then resolved by sodium dodecyl sulphate–polyacrylamide gel electrophoresis (SDS–PAGE) and analyzed by western blot using anti-Dyrk1a and anti-Dscam antibody. Note the band of 85 kDa expected for the Dyrk1a protein and the 250 kDa band expected for Dscam protein. No cross-reaction was found with the IgGs.

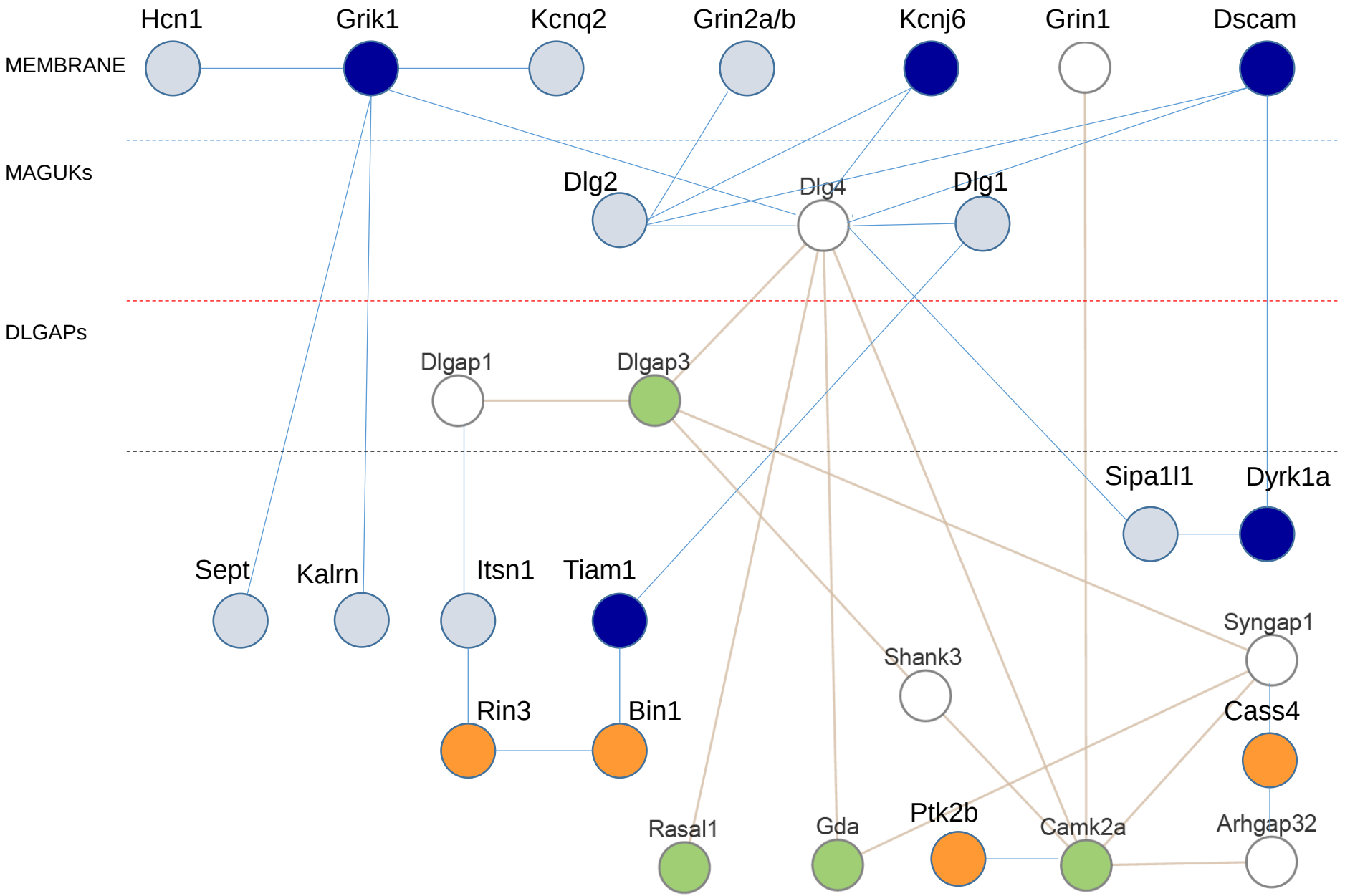
Hcn1
Grik1
Kcnq2
Grin2a/b
Kcnj6
Grin1
Dscam
MEMBRANE
MAGUKs
DLGAPs
Dlg2
Dlg4
Dlg1
Dlgap1
Dlgap3
Sipa1l1
Dyrk1a
Sept
Kalrn
Itsn1
Tiam1
Syngap1
Shank3
Rin3
Bin1
Cass4
Rasal1
Gda
Ptk2b
Camk2a
Arhgap32

Figure 8.

Figure 8. Protein-protein interactions in the three layers of dendritic spine PSD: enrichment in proteins encoded by either HSA21 or LOAD-GWAS genes

Schematic representation of synaptic protein-protein interactions performed by yeast-two-hybrid, with the three layers of dendritic spine PSDs indicated (membrane; MAGUKs, DLGAPs). HSA21-encoded proteins are represented as dark blue circles. LOAD-GWAS encoded proteins are represented by dark orange circles.

A

```
P59020       DSCR9_HUMAN         1   MGRICPVNSRARRLRARPGRPSGDSLPYHQLQGGAPRLWSPDPGRPAAYRRAHVCDVTAP   60
P59021       DSCR9_PANTR         1   MGRICPVNSRARRLRARPGRPSGDSLPYHQLQGGAPRLWSPDPGRPAAYRRAHVCDVTAP   60
Q4R745       Q4R745_MACFA        1   MTQQ----S-------------------KTQMKQDEEWAAQ---QVKLHHVTDCSPGME   33
A0A0D9R839   A0A0D9R839_CHLSB    1   MGRICPVNSRTRRLRASPGCPSGDSPPRHQLQGGVPGLGSPDPGSPAAYRRSM-SACNSP   59
                                     * :     *                  : *       : :    .  ::   .

P59020       DSCR9_HUMAN        61   RWGST-SRQGEGAVLQRMLGRRAPPSWS---RDHAYSRRGWENAALFLNRKRKQEGTENT  116
P59021       DSCR9_PANTR        61   RWGST-SRQGEGAVLQRMLRRRAPPSWS---RDHAYSRRGWENVALFLNRKRKQEGTENT  116
Q4R745       Q4R745_MACFA       34   RWRGAQR-DGQAPGKM-----------------DFFP-------------QTSNATNT   60
A0A0D9R839   A0A0D9R839_CHLSB   60   RWGSASSRQGEGAVLPPMLRRRGQSSWSARARDHAYSPRGWENAALSLNRKRKQEGTENT  119
                                     ** .:   :*:.                     :                 : ..: **

P59020       DSCR9_HUMAN       117   SICCRPESALACGGNLSPQFLKKVIQIQTQELW                          149
P59021       DSCR9_PANTR       117   SICCRPESALACGGNLSPQFLKKVIQIQTQELW                          149
Q4R745       Q4R745_MACFA       61   SILTRSL-------------------------                          67
A0A0D9R839   A0A0D9R839_CHLSB  120   GICCRPESALACGGNLSPQFFEKVIRIHTQELW                          152
                                     .*  *
```

B

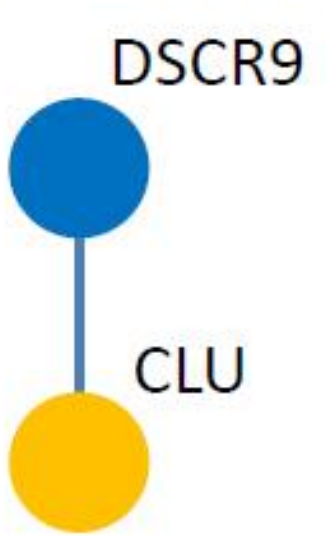

C

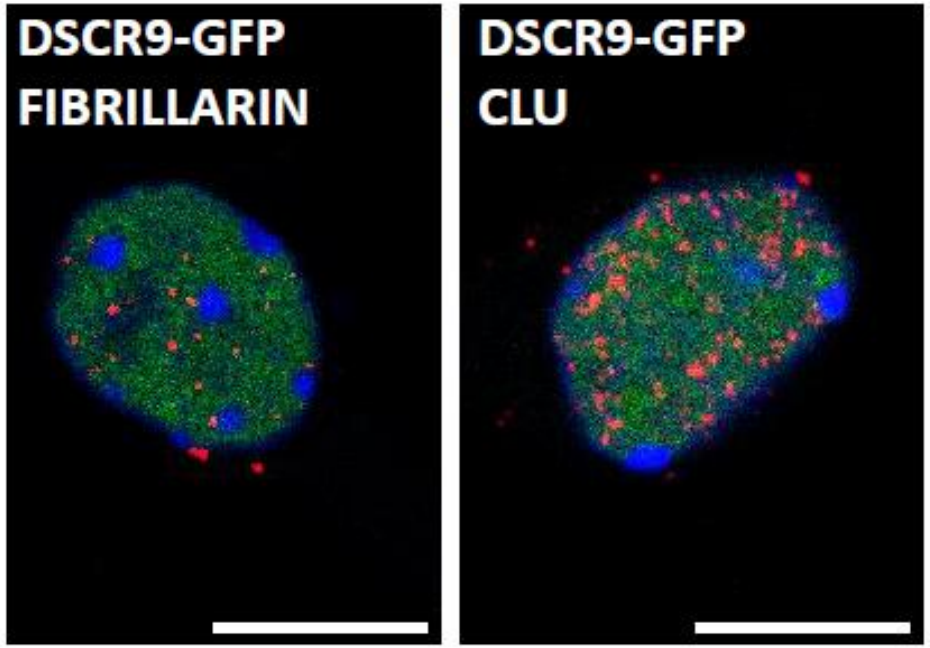

Supplementary Figure S1

Supplementary Figure S1. Interactions of HSA21 DSCR9 with CLU involved in LOAD

(**A**) **Protein multiple sequence alignment of DSCR9 proteins for different species**
We used UnitProt Align for Homo sapiens (Human), Pan troglodytes (Chimpanzee), Macaca fascicularis (Crab-eating macaque) and Green monkey (Cercopithecus sabaeus) sequences, respectively. DSCR9 is specific for human and non-human primates.
(**B**). Schematic representation of protein-protein interactions identified by yeast-two-hybrid using a human brain library. Dark blue circles indicate HSA21 encoded proteins; orange circle indicates a LOAD-related protein. (**C)**. *In situ* PLA on primary cortical neurons transfected at DIC5 and fixed 48 hours later at DIC7 (red fluorescence) using anti-GFP and anti-Clu antibodies. PLA using anti-GFP and anti-Fibrillarin antibodies were performed as a negative control. Green fluorescent protein was visualized on green channel and nuclear bodies were labelled using Topro3 (blue fluorescence).

A

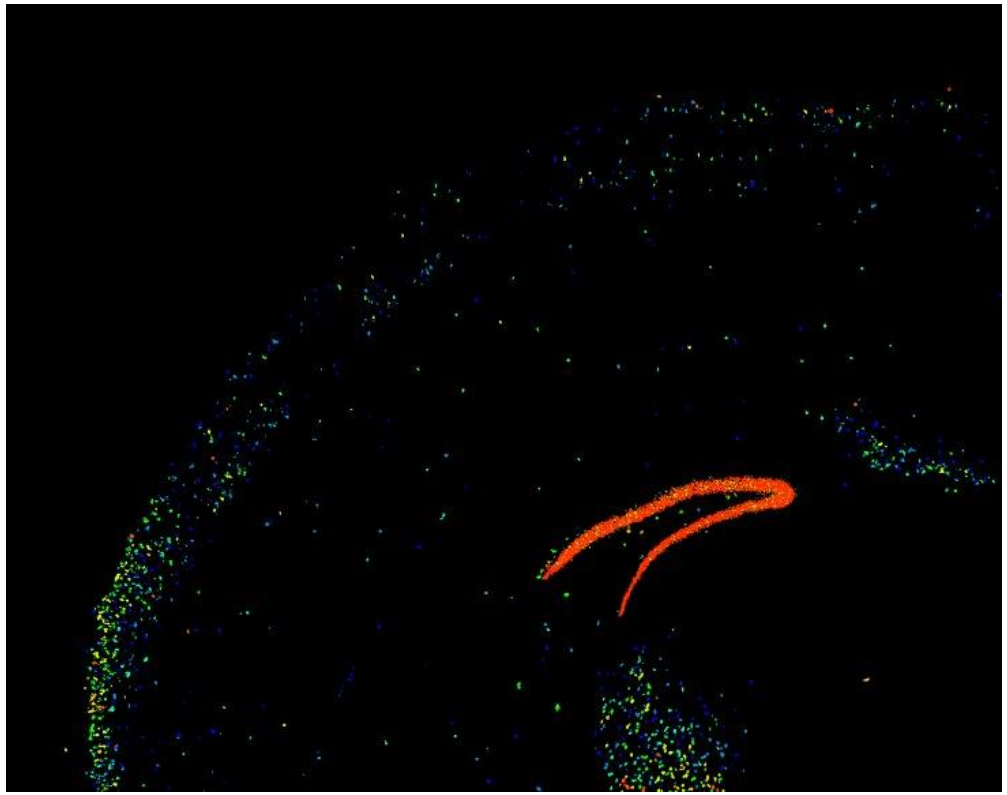

B

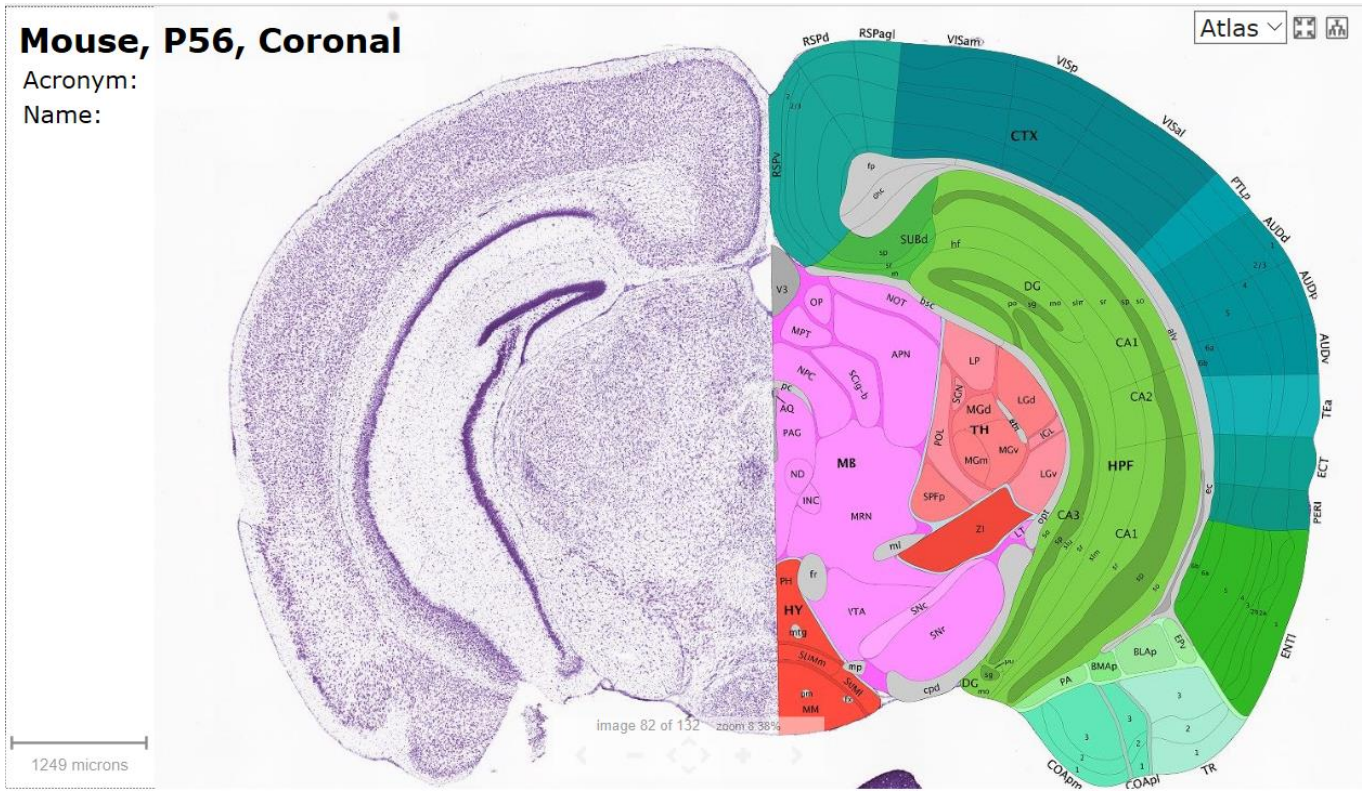

Supplementary Figure S2

Supplementary Figure S2. Specific expression of *Tiam1* in mouse brain

Tiam1 expression is restricted to dentate gyrus in adult mouse brain.

(**A**) In situ hybridization. (**B**). Nissl data and schematic illustration of the different brain regions for a coronal section (Data from Allen Brain Institute).